T.C.
YALOVA UNIVERSITY
INSTITUTE OF GRADUATE STUDIES

POLYMER MATERIALS ENGINEERING DEPARTMENT
POLYMER ENGINEERING PROGRAMME

ELECTROMECHANICAL SENSING PROPERTIES OF FLEXIBLE ELECTRONICS FROM FUNCTIONAL POLYMER NANOCOMPOSITES

M.Sc. THESIS

MUKADDES ŞEVVAL ÇETİN

ADVISOR: Assist. Prof. Dr. HATİCE AYLİN KARAHAN TOPRAKÇI

YALOVA
APRIL 2022

T.C.
YALOVA UNIVERSITY
INSTITUTE OF GRADUATE STUDIES

POLYMER MATERIALS ENGINEERING DEPARTMENT
POLYMER ENGINEERING PROGRAMME

ELECTROMECHANICAL SENSING PROPERTIES OF FLEXIBLE ELECTRONICS FROM FUNCTIONAL POLYMER NANOCOMPOSITES

M.Sc. THESIS

MUKADDES ŞEVVAL ÇETİN

195101004

ADVISOR: Assist. Prof. Dr. HATİCE AYLİN KARAHAN TOPRAKÇI

YALOVA
APRIL 2022

ETHICAL STATEMENT

In this thesis study, which I prepared based on Yalova University Institute of Graduate Studies Thesis Writing Rules; the data, information, and documents I have been presented in the thesis were obtained with the insight of academic and ethical rules; all the information, documents, evaluations, and results are presented based on scientific ethical and moral rules; all the references used in the thesis were cited; no changes were made in the data presented in the thesis and the study presented in the thesis is original. In the case of proving the contrary, I undertake and declare that I accept any legal responsibility.

Mukaddes Şevval ÇETİN

PREFACE

I dedicate this study,

To my parents Naime and Cengiz Çetin, who always support me unconditionally. I am thankful for their trust and prayers. They always taught me to be right and fair person and I am lucky to be their daughter.

To my little sister Hilal Aleyna Çetin who always makes me feel her love and support. I am lucky to be her elder sister and grown with her. I am thankful for her inspiration and encouragement.

To my cousin Ela Dede, who loves me with her heart. I always feel her small hands with me. She is the meaning of pure love in my life.

I express my thankful to my lovely advisor, Dr. Hatice Aylin Karahan Toprakçı. I feel very honored to be her student. I thank her for her trust, guidance, support, and humanity.

I want to thank to Dr. Ozan Toprakçı who mentored me. His guidance and help are very valuable to me.

I am very proudful being a member of Toprakci Research Group.

I would like to thank TUBITAK and Yalova University for their financial supports;

-"Electromechanical Sensing Properties of Flexible Electronics from Functional Polymer Nanocomposites" project was supported by TUBITAK 2210-C National Graduate Scholarship Program in High Priority Technological Areas

-Yalova University, BAP (Scientific Research Project) Project No: 2020/YL/0013, "Electromechanical Sensing Properties of Flexible Electronics from Functional Polymer Nanocomposites"

April - 2022 Mukaddes Şevval ÇETİN

TABLE OF CONTENTS

SYMBOL AND ABBREVIATION LIST

SYMBOLS

R	**:**	Resistance
R_0	**:**	Initial resistance
$\Delta R/R_0$	**:**	Fractional resistance change
ε	**:**	Strain
l	**:**	Length
l_0	**:**	Initial length

ABBREVIATIONS

CB(s)	**:**	Carbon Black (Particles)
CNFs	**:**	Carbon Nanofibers
CNT(s)	**:**	Carbon Nanotube(s)
DMF	**:**	Dimethylformamide
E-textile	**:**	Electronic Textile
GF	**:**	Gauge Factor
GO	**:**	Graphene Oxide
ICP(s)	**:**	Inherently Conductive Polymer(s)
KNF	**:**	Buhar Biriktirme Yöntemi ile Üretilmiş Karbon Nanofiber
KS	**:**	Karbon Siyahı
OBC	**:**	Olefin Block Copolymer
PDMS	**:**	Polydimethyl Siloxane
rGO	**:**	Reduced Graphene Oxide
SBS	**:**	Poly(styrene-butadienestyrene)
SCF	**:**	Supercritical Fluid
S/EB	**:**	Styrene to Ethylene-butylene Ratio/Stirenin Etilen-bütilene Oranı
SEBS	**:**	Poly(styrene-b-(ethylene-co-butylene)-b-styrene)/Poli[stiren-b-(etilen-ko-bütilen)-b-stiren]
TPEs	**:**	Thermoplastic Elastomers
TPU	**:**	Thermoplastic Polyurethane
VGCNF(s)	**:**	Vapor Grown Carbon Nanofiber(s)

TABLE LIST

FIGURE LIST

ELECTROMECHANICAL SENSING PROPERTIES OF FLEXIBLE ELECTRONICS FROM FUNCTIONAL POLYMER NANOCOMPOSITES

ABSTRACT

Polymers that are lightweight, easily processable, and have different morphological, thermal, mechanical, and electrical properties, are generally preferable for various applications such as electronics, automotive interiors, outdoor products, biomedical, etc. thanks to their tunable properties. With the incorporation of filler/additive materials, some properties of the polymeric matrix can be changed. For instance, for the applications those require electrical conductivity, electrically conductive polymer composites are fabricated with the addition of conducting filler material into the insulating polymer matrix. In this case, not only filler properties but also matrix properties are of significance in terms of the final properties of the conductive composites. In this work, to observe the effect of filler and matrix type on piezoresistive sensing performance, different nanocomposites were prepared. Two different poly[styrene-b-(ethylene-co-butylene)-b-styrene] (SEBS) with different block ratios (styrene to ethylene-butylene ratio (S/EB): 13/87 and 19/81) and three different filler systems were used including carbon black (CB), vapor grown carbon nanofibers (VGCNFs), and mixture of CB and VGCNF (VGCNF:CB = 1) at the filler concentration between 0.5 to 6.5 wt% for the first time in the literature. In the first step of this study, flexible conductive polymer composites were fabricated and their morphological, electrical, mechanical properties and piezoresistive sensing performance were investigated depending on filler type, filler concentration, and matrix type. Regarding to the percolation behavior, composite sets were found to be used as strain sensors. However, the sensitivity of hybrid filler-based nanocomposites was higher that could be given as the novelty of the study. The nanocomposite with 3.5 wt% CB-VGCNF hybrid filler showed the gauge factor (GF) around 333 that was one of the highest sensitivity obtained for SEBS based hybrid nanocomposites in the literature. The reason was the unique conductive network formation with the addition of VGCNF into CB. Not only decrease in percolation concentration was observed compared to CB-filled nanocomposites but also formation of new unique conductive network morphology was achieved that was highly sensitive to strain deformation because of additional junctions between low and high aspect ratio fillers. In the final step of the study, a textile-based sensor was fabricated from the hybrid nanocomposites by coating on the fabric surface, and its morphological, and electromechanical properties were also characterized. The GF of the textile-based piezoresistive strain sensor was found around 108 that was also reported for the first time in the literature.

Keywords: Piezoresistive sensor, Flexible electronic, Strain sensor, Thermoplastic elastomer, Electrically conductive nanocomposite

FONKSİYONEL POLİMER KOMPOZİTLERDEN ÜRETİLEN ESNEK ELEKTRONİKLERİN ELEKTROMEKANİK ALGILAMA ÖZELLİKLERİ

ÖZET

Hafif, kolay işlenebilen, farklı morfolojik, termal, mekanik ve elektriksel özelliklere sahip olan polimerler, ayarlanabilir özellikleri sayesinde genellikle elektronik, otomotiv iç mekanları, dış mekan ürünleri, biyomedikal vb. gibi çeşitli uygulamalarda tercih edilmektedir. Dolgu/katkı malzemelerinin eklenmesi ile polimer matrisin bazı özellikleri değiştirilebilmektedir. Örneğin, elektriksel iletkenlik gerektiren uygulamalar için yalıtkan polimer matrise iletken dolgu malzemesi eklenmesi ile elektriksel olarak iletken polimer kompozitler üretilmektedir. Bu durumda iletken kompozitlerin son özellikleri açısından sadece dolgu özellikleri değil aynı zamanda matris özellikleri de önemlidir. Bu çalışmada, dolgu ve matris türünün piezorezistif algılama performansı üzerindeki etkisinin gözlemlenmesi için farklı nanokompozitler hazırlanmıştır. Literatürde ilk kez, farklı blok oranlarına sahip iki farklı poli[stiren-b-(etilen-ko-bütilen)-b-stiren] (SEBS) (stirenin etilen-bütilene oranı (S/EB): 13/87 ve 19/81) ve karbon siyahı (KS), buhar biriktirme yöntemi ile üretilmiş karbon nanofiberler (KNF) ve KS ve KNF karışımı (KNF:KS = 1) olmak üzere üç farklı dolgu ağırlıkça %0.5-6.5 konsantrasyonlarında kullanılmıştır. Bu çalışmanın ilk aşamasında, esnek iletken polimer kompozitler üretilmiş ve dolgu türüne, dolgu konsantrasyonuna ve matris türüne bağlı olarak kompozitlerin, morfolojik, elektriksel, mekanik özellikleri ve piezorezistif algılama performansları incelenmiştir. Perkolasyon davranışı göz önünde bulundurularak kompozitlerin uzama sensörleri olarak kullanılabildiği tespit edilmiş olsa da hibrit dolgu içeren nanokompozitlerin hassasiyetinin daha yüksek olması çalışmanın özgülüğü olarak verilebilir. Ağırlıkça %3.5 KS-KNF hibrit dolgulu nanokompozit, SEBS içeren hibrit nanokompozitler için elde edilen hassasiyet değeri (GF) yaklaşık olarak 333 civarındadır ve bu değer literatürdeki hibrit dolgulu SEBS piezorezistif sensörlerde elde edilen yüksek değerlerdendir. Bunun nedeni, KNF'nin KS'ye eklenmesiyle oluşan benzersiz iletken ağ oluşumudur. KS dolgulu nanokompozitlere kıyaslandığında sadece perkolasyon konsantrasyonunda azalma gözlemlenmemiş, aynı zamanda düşük ve yüksek aspek oranlı dolgu maddeleri arasındaki ek bağlantılardan dolayı uzamaya karşı oldukça hassas olan yeni, benzersiz iletken ağ morfolojisinin oluşumu sağlanmıştır. Çalışmanın son aşamasında, hibrit nanokompozitler kumaş yüzeyine kaplanarak tekstil içeren sensör üretilmiş ve morfolojik ve elektromekanik özellikleri incelenmiştir. Tekstil esaslı piezorezistif uzama sensörünün gage faktörü yaklaşık 108 bulunmuş ve bu da literatürde ilk kez rapor edilmiştir.

Anahtar Kelimeler: Piezorezistif sensor, Esnek elektronik, Uzama sensörü, Termoplastik elastomer, Elektriksel iletken polimer nanokompozit

1. INTRODUCTION

The long history of flexible electronics started with flexible solar cell arrays made from thin single crystal silicon in the 1960s. In those days, all thin materials were called 'flexible'[1]. With improvements and research, flexible electronics have gained more importance. Several sectors including automotive, biometrics, mobile and smart devices, (TVs, monitors, screens, sensors, etc.) need flexible electronics. The easiest way to produce flexible electronics is to use polymers. Since polymer-based flexible electronics are lightweight, bendable, easily processable, and have dimensional stability with tunable properties, it is possible to use them in a wide range of applications. Sensors that transform the input signal into electrical response are one of the specialized areas of flexible electronics. There are number of ways to classify the sensors. The contact or non-contact sensors are the kinds of sensors. According to the reference point, they can be called absolute or relative sensors. Sensors can measure properties such as strain, pressure, temperature, and the classification can be done based on measured property. There are sensors that work based on capacitive, inductive, optical, chemical, piezoelectric, and piezoresistive mechanisms. For instance, piezoresistive strain sensors, which monitor the resistance change under strain and measure applied strain, can be flexible electronic components of the electronic textiles (e-textiles). The most important requirement to produce this type of sensor is its electrical conductivity. In the fabrication of sensors, generally, polymers are chosen. Regarding electrical conductivity, polymers can be classified as; inherently conductive polymers (ICPs), and insulating polymers. To enhance the electrical conductivity of the polymer matrix, polymer composites can be fabricated with the addition of electrically conductive filler materials. These are generally carbon-based materials such as carbon black (CB), carbon nanofiber (CNF), carbon nanotube (CNT), graphene, graphene oxide (GO), and reduced graphene oxide (rGO). Since repeatability, high resilience, and high sensitivity are significant requirements, thermoplastic elastomers (TPEs) are commonly preferred for matrix material. TPEs show high resilience, flexibility, repeatability and they possess both thermoplastic and elastomeric material properties. With the combination of these materials, superior electrical conductivity, and mechanical properties can be obtained. The sensitivity of

the sensor can be tuned depending on the filler properties such as filler loading, particle size, geometry, aspect ratio, surface area, and porosity.

In this study, the production of thermoplastic elastomer-based piezoresistive strain sensors and characterization of their morphological, electrical, mechanical, and electromechanical properties were carried out. The strain sensors were designed with carbon black, vapor grown carbon nanofibers, and hybrid (CB and VGCNF mixture) fillers, fabricated based on solution casting and compression molding, and coated onto the elastomeric fabric. The most important goal of the study was to analyze the effects of hybrid filler material on all these properties, especially sensing properties. The content of the study can be given as below:

Chapter 1. Introduction; In this chapter, general information about piezoresistive strain sensors is given.

Chapter 2. Literature; In this chapter, recent literature review about thermoplastic elastomer-based piezoresistive strain sensors is given.

Chapter 3. Materials and Methods; In this chapter, materials and methods used for fabrication and characterization of nanocomposites and textile sensors are given

Chapter 4. Results; In this chapter, evaluation of the results obtained from nanocomposites and textile based sensor are given.

Chapter 5. Conclusions and Future Suggestions; In this chapter, conclusions and suggestions for future studies are given.

2. LITERATURE

2.1 Sensors

The system used for the transformation of signal into the electrical response is called sensor[2]. The input signal can be in different forms such as mechanical, chemical, optical, and others, while voltage and current can be the type of output signal [2].

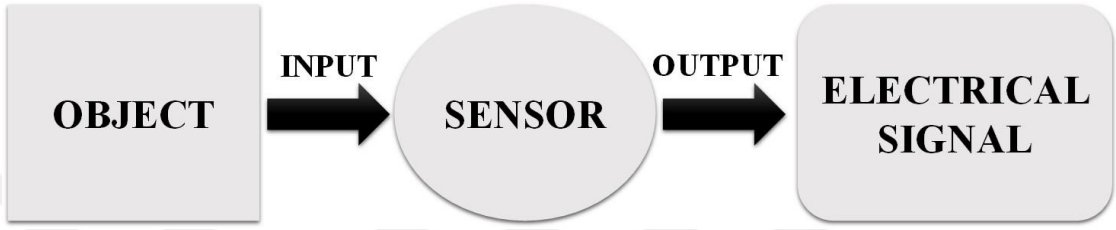

Figure 2.1. Mechanism of the sensors [3]

There are many types of sensors those can be classified regarding their sensing mechanisms such as capacitive, optical, piezoelectric, and piezoresistive sensors etc. Since piezoresistive sensors were developed in this study, detailed information will be given the following sections.

2.1.1 Piezoresistive sensors and piezoresistive strain sensors

Piezoresistive sensors are one of the mostly used types of the sensors. The mechanism is based on piezoresistance. The piezoresistance term expresses the change in electrical resistance of the material under deformation [4–6]. Stretching, bending, compression, temperature change, gas, or chemical exposure can be given as some reasons for micro or large scale deformation [5, 7].

One of the specified types of sensors is the piezoresistive strain sensors. For strain sensors, under different strain levels, change in electrical signal is measured [8]. In the literature, elastomers (isoprene, polydimethyl siloxane (PDMS)) [9–13], and thermoplastic elastomers (thermoplastic polyurethane (TPU), poly(styrene-butadienestyrene) (SBS), poly(styrene-b-(ethylene-co-butylene)-b-styrene) (SEBS)) [14, 15, 16–23, 24–26] are the most commonly used materials. Since electrical signal is measured, electrical conductivity of the system is the most important requirement. With the addition of electrically conductive fillers to electrically insulating polymer

matrixes such as isoprene, PDMS, TPU, SBS, SEBS, the required electrical property is obtained.

Piezoresistive sensor should have some basic properties. One of them is the response behavior. Generally, two different responses can be observed for piezoresistive strain sensors depending on the polymer type, filler properties, filler concentration, sensor production method, and strain level. With the applied strain, resistance increases due to break-down of conducting network and the behavior called "Positive Piezoresistance" (Figure 2.2) [3, 27].

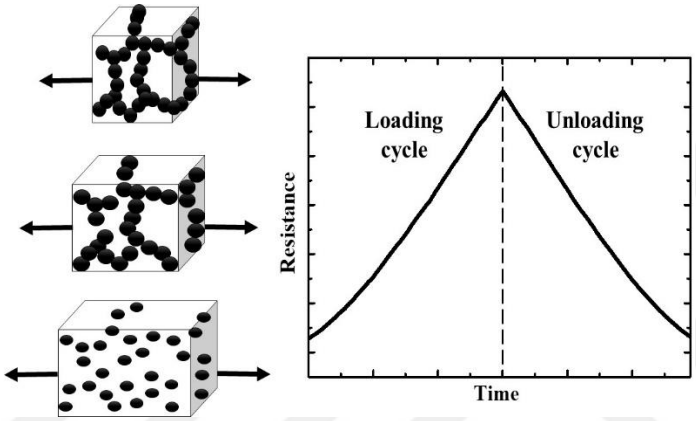

Figure 2.2. Illustration of positive piezoresistance [3]

The other behavior is called "Negative Piezoresistance". In this case, fillers come close to each other and new network formations can be seen with the applied strain. Consequently, resistance decreases (Figure 2.3) [3, 27].

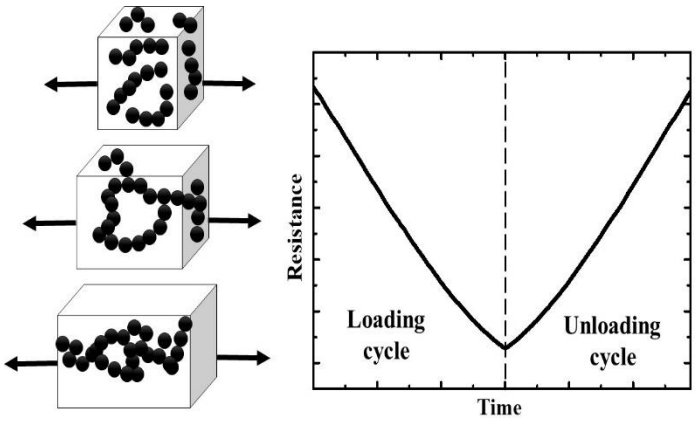

Figure 2.3. Illustration of negative piezoresistance [3]

It is also important to obtain meaningful response under working range. The linear character under test conditions is preferred for the sensors.

Besides, the cyclic behavior is important to investigate the piezoresistive properties of the sensors. To analyze the cyclic behavior of the sensor, at least 10 cycles are performed. The behavior shows the recoverability of the system. The material should return to its original shape after one cycle is performed and the response should be repeatable for all cycles.

Another important concept for the polymer based piezoresistive strain sensors is the sensitivity. Sensitivity depends on the change in resistance under given strain level. This term is given by "Gauge Factor" (GF). GF of a polymer-based piezoresistive composite is dependent on resistance and strain of the sample and is calculated with the following equation (Eq.1);

$$GF = \frac{\Delta R/R_0}{\varepsilon_{axial}} \tag{2.1}$$

, where R is the resistance, R_0 indicates the initial resistance value of the sample and $\Delta R/R_0$ is defined as the fractional resistance change. ε is symbolized strain and equals to (Eq.2);

$$\varepsilon = \frac{l - l_0}{l_0} \tag{2.2}$$

, where l and l_0 express the length and initial length of the sample, respectively. The increasing number of GF means that the sensitivity of the sensor increases. For the piezoresistive strain sensor, the sensitivity of the sensor is directly related to the resistance change under applied strain [27–30].

2.2 Electrically Conductive Polymer Composites

Polymer composites, which consist of the polymeric matrix and filler material, are highly used in the sensor applications, circuit components, batteries, and fuel cells because of their lightness, flexibility, ease of production. Depending on the requirements of the nanocomposite, different matrixes and fillers can be used. In this case, it is important to produce an electrically conductive polymer composite since most of the polymers are electrically insulators [31]. Carbonaceous fillers such as carbon black (CB) [25, 32], carbon nanofiber (CNF) [21, 26], carbon nanotube (CNT) [17, 22, 33, 34], graphene and its derivatives (graphene oxide (GO), reduced graphene oxide (rGO)) [10, 35] can be used to enhance the electrical conductivity of the insulating polymer matrix and semi-conducting, or conducting materials can be

obtained. The electrical conductivity and monitored electrical response from polymer composite is changed with the addition of filler material depending on the its amount, particle size, shape, aspect ratio, surface area, porosity [36, 37]. The situation explains with percolation theory and expressed as (Eq.3) [38]**;**

$$\sigma = \sigma_1 (f - f_c)^{\alpha} \quad (2.3)$$

where, percolation threshold is symbolized with f_c, while f is defined as the volume fraction of filler. σ and σ_1 express the conductivity of polymer composite and filler material, respectively. According to the theory, three different regions were observed in polymer composites (Figure 2.4). The first region is called insulation. In the region, $f<f_c$ and the filler materials are far away from each other. In the insulation region, the significant change in volume resistivity is not observed since the electrical network doesn't form. With the increase in the amount of filler material, the conductive phase forms conductive network in the matrix, and the remarkable change in volume resistivity can be seen. In third region which is above the percolation region, important change is not observed even the filler ratio is increased and the region is called saturation region [38–42].

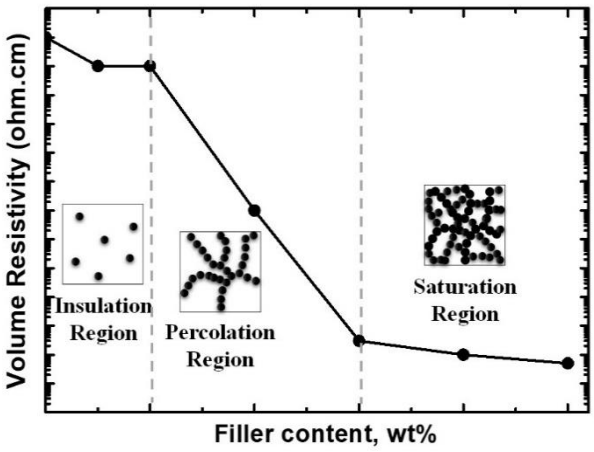

Figure 2.4. Illustration of percolation regions [38, 40, 43–48]

2.3 Thermoplastic Elastomer Based Piezoresistive Strain Sensors

For strain sensors, sensitivity, repeatability, flexibility, high resilience are important points to obtain meaningful and linear cyclic behavior. Elastomers are highly used in this area. Especially, TPEs, which can be processed like thermoplastic materials and contained physical crosslinks by elastomer domains, are preferred materials because

of their superior mechanical properties such as high flexibility, good resilience, high bendability, and high stretchability.

In the literature, there are many studies about TPE-based piezoresistive strain sensors. In these studies, TPU [32, 49, 50], SBS [23], and SEBS [16, 20, 21, 24, 25] were used as polymeric matrixes. Carbon black, carbon nanofibers, carbon nanotubes, graphene, and the mixture of different fillers were used as the electrically conducting filler material. In the aspect of these studies, it can be understood that generally carbon-based filler materials were used. With their high conductivity, inert structure, different form (geometry, aspect ratio, size), the sensor properties can be tuned easily. The other outcome of the literature is related to the production methods. Generally, solution casting [17, 21, 26, 36] and melt processing [20, 24, 25] are preferred.

In this section, piezoresistive sensors with carbon black and carbon nanofiber filled thermoplastic elastomer were investigated.

2.3.1 Piezoresistive strain sensors with carbon black filled thermoplastic elastomers

In this part, previous studies related to the strain sensing properties of carbon black-filled thermoplastic elastomer-based composites were investigated. SBS, SEBS, and TPU were commonly used thermoplastic elastomers in these studies. Composites, consisting of different filler concentrations up to 50 wt%, were generally fabricated by the extrusion and solvent-casting method. The sensors were used in the form of fiber or film.

One of the studies was carried out by Cochrane et al. [23]. CB/SBS composites were produced in different ways; melt mixing and solvent casting method. In the melt mixing process, nine different composites were fabricated with volume ratios of 3.6, 5.4, 7.3, 9.2, 11.1, 15.0, 19.1, 23.3, and 27.6 %. The solvent-casted composites consisted of 7.3, 11.1, 19.1, and 27.6 vol % of CB. A digital image of the sensor, integrated onto nylon fabric, can be seen in Figure 2.5 [23].

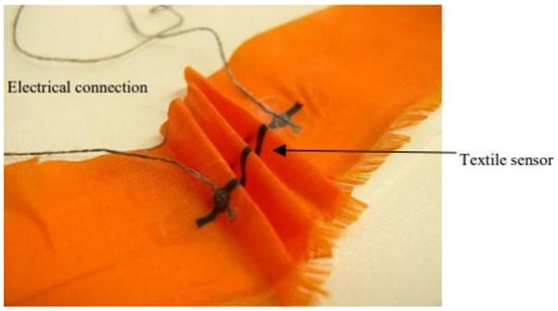

Figure 2.5. Digital image of fabric sensor, produced by solvent casting method and consisting of 27.6 vol% [23]

Percolation region for both composites was observed around 7 vol % (Figure 2.6). At the same filler content, it was shown that solvent-casted samples had lower resistivity values [23].

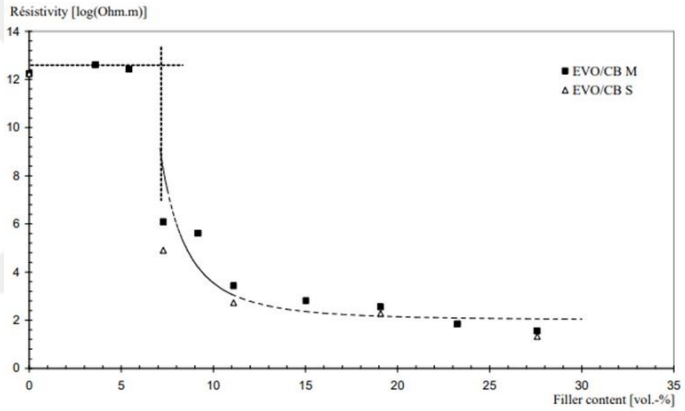

Figure 2.6. Electrical resistivity of melt mixed and solvent-casted samples [23]

27.6 vol% CB/SBS solvent casted composite was evaluated as a strain sensor. In Figure 2.7 normalized electrical resistance depending on different strain levels was given. At 15% and higher strain levels, the sensor showed an almost linear behavior [23].

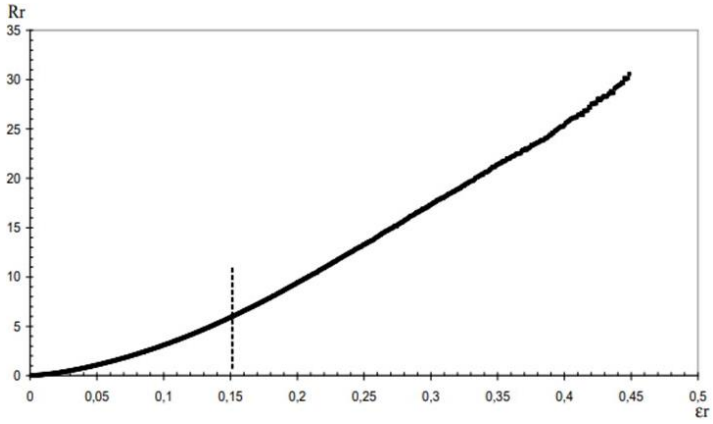

Figure 2.7. Normalized electrical resistance value at different strain values [23]

In summary, strain sensors, consisting of SBS and CB, were produced by two different methods. The percolation threshold for both composites was determined around 7 vol% of filler loading. It was reported that the sensor showed a linear behavior above 15% strain. The important contribution of the study was to investigate the effect of environmental conditions. It was reported that the behavior of the sensor was highly affected by humidity. On the other hand, morphological images of the composites and cyclic behavior of the sensors were not given [23].

Mattmann et al. [24] fabricated a strain sensor for textile applications. Mechanical, piezoresistive, aging, and washability properties of CB-filled SEBS composites were investigated. CB/SEBS with a thickness of 315 μm can be seen from Figure 2.8 [24].

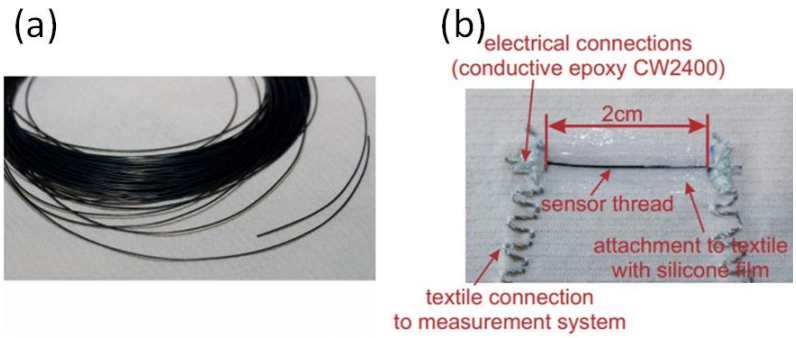

Figure 2.8. (a) Extruded CB/SEBS composite, and (b) sensor with electrodes [24]

50 wt% CB/SEBS was chosen for the electro-mechanical analysis. The test speed was adjusted to 200 mm/min. In Figure 2.9, the sensor was pre-stretched and deformed up to 80%. Then, deformation was decreased gradually down to 20%. It can be seen that similar behavior was obtained [24].

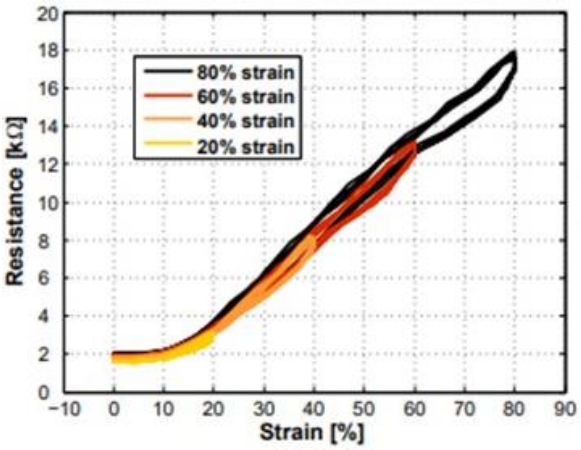

Figure 2.9. The resistance change of pre-stretched sensor depending on decreasing strain levels [24]

In Figure 2.10, the sensor wasn't pre-stretched and deformed at 20%. Then, deformation was increased gradually up to 100%. It can be seen that different responses were obtained at different strain levels [24].

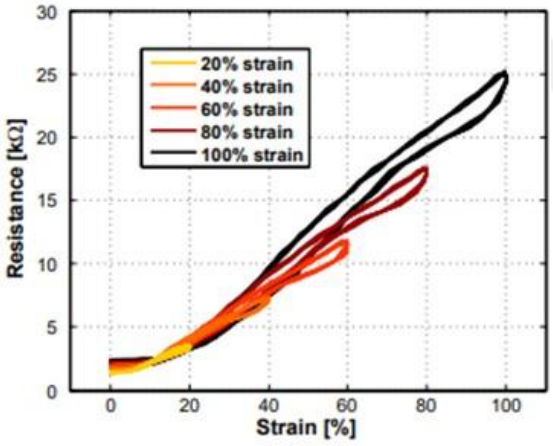

Figure 2.10. The resistance change without a pre-stretched sensor depending on increasing strain levels [24]

It was also investigated the effect of test speed on the piezoresistive properties of the sensor. The test speed was varied between 50 and 600 mm/min (Figure 2.11). Resistance change increased with the increasing test speed [24].

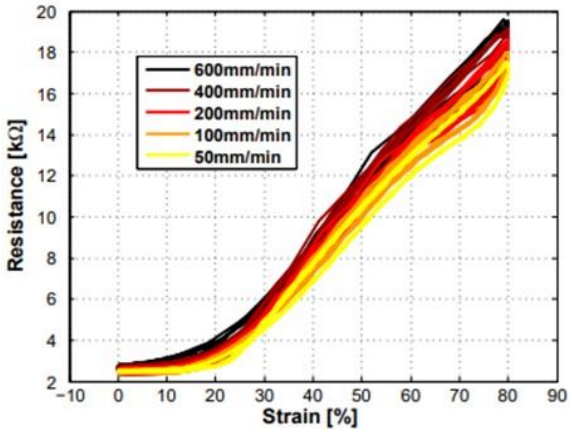

Figure 2.11. The resistance change depending on test speed [24]

As a summary, Mattmann et al. developed and characterized a textile-based piezoresistive textile sensor. The composites with different filler ratios were fabricated in the fiber morphology and 50 wt% CB/SEBS was selected to investigate the sensing properties. The sensor, pre-stretched or not, was shown to perform at higher strain levels. After aging and washability tests sensor behavior remained its stability. This study was one of the first ones in terms of considering electro-mechanical history [24].

In another study, Clemens et al. [25] studied the effect of hardness of SEBS on piezoresistance. 3 different SEBS matrixes were used. 30-58 wt% CB was added into the matrix. The fibers with 300 µm thickness were produced via extrusion (Figure 2.12). In order to investigate the piezoresistive properties, 30 wt% filler loading was chosen for all SEBS. The lowest relaxation behavior was observed for the SEBS with the highest hardness value [25].

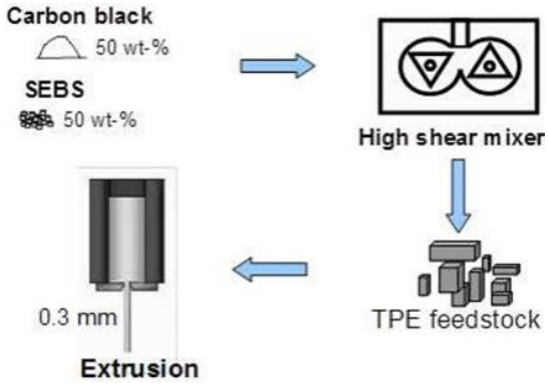

Figure 2.12. Preparation of CB/SEBS composite [25]

For further investigations, the hardest SEBS was chosen. Cyclic behavior was analyzed as a function of filler loading that varied from 30-58 wt% at 13-30% strain levels. It was reported that stability was obtained above 45 wt% CB concentration (Figure 2.13) [25].

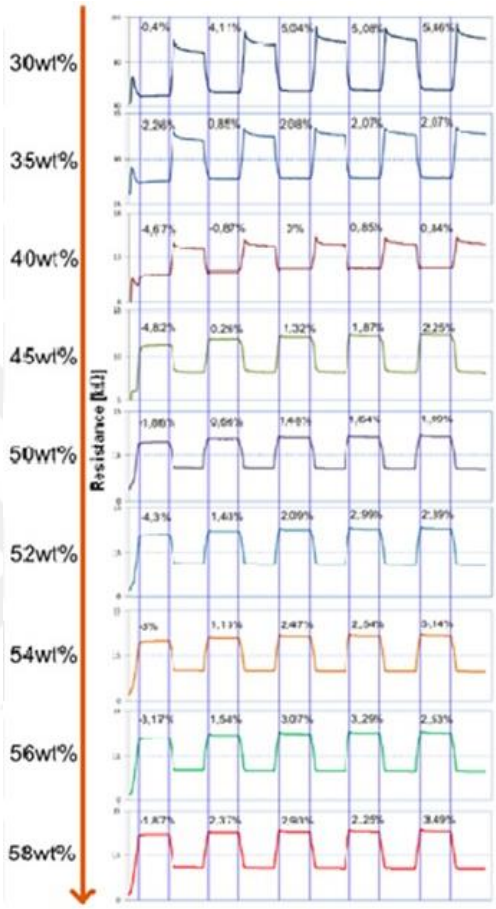

Figure 2.13. Cyclic behavior of the hardest SEBS depending on the filler ratio (at 13-30% strain levels) [25]

As a summary of the study, Clemens et al. produced CB-filled SEBS sensors with different hardness via using an extruder. SEBS, having the highest hardness value, was chosen for cyclic analysis. It was concluded that sensor stability was obtained at higher than 45 wt% filler loading. Although the study was significant in terms of using various SEBS matrixes, percolation graphs and morphology of the composites were not given [25].

In another study, Melnykowycz et al. [16] produced a strain sensor in the fiber form. The properties of CB/SEBS sensor were compared with different commercial monofilaments, having various fiber diameters. In the study, Empa fibers with a diameter of 0.3 and 2 mm were produced by using a capillary rheometer. Some properties (thickness and electrical) can be seen in Table 2.1 [16].

Table 2.1. Thickness and electrical properties of commercial and produced monofilaments [16]

Monofilament Type	Dia. (mm)	Ω/mm	Ω.mm
Images SI	1.72	13.62	31.65
Merlin Systems	2.00	15.20	47.75
Empa	2.00	1.03	3.01
Empa	0.30	36.00	2.54

In Figure 2.14a and b., normalized resistance depending on the strain (15-30 %) can be seen for Empa and the other monofilaments. All samples showed positive piezoresistance. It was shown that commercial monofilaments had almost the same cyclic behavior (Figure 2.14b) and the sample with a lower diameter showed higher resistance change. Empa, having the lowest diameter, showed the highest resistance change, compared with other commercial monofilaments. GF values can be seen from Table 2.2. The highest GF was obtained by using Empa filament with a diameter of 0.3 mm [16].

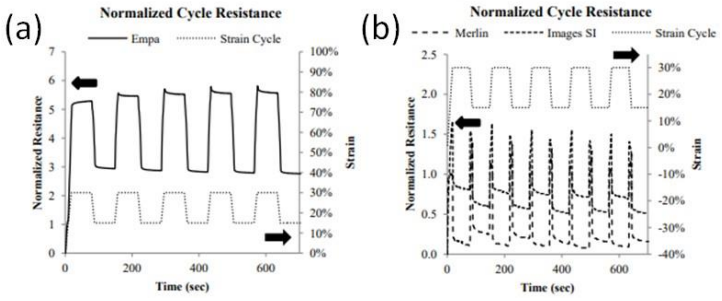

Figure 2.14. At 15-30% strain, cyclic behavior of (a) Empa monofilament, and (b) commercial monofilaments [16]

Table 2.2. GF of monofilament depending on cycle number at 15 and 30% strain [16]

30% Strain						
Cycle	**1**	**2**	**3**	**4**	**5**	**Avg.**
Merlin	0.35	0.35	0.35	0.22	0.31	0.32
Images SI	2.66	2.52	2.48	2.39	2.34	2.48
Empa 0.3 mm	17.61	18.19	18.40	18.50	18.54	18.25
15% Strain						
Merlin	1.67	1.32	0.88	1.05	1.05	1.19
Images SI	3.96	3.78	3.42	3.51	3.42	3.62
Empa 0.3 mm	19.61	19.13	18.82	18.58	18.38	18.90

As a summary, Melnykowycz et al. studied the comparison of commercial monofilament and CB/SEBS monofilament with different diameters. The study is useful in terms of investigating diameter effect on the sensing properties. The highest stability was obtained Empa monofilament, consisting of CB/SEBS, with the lowest diameter. On the other hand, there is no information about the morphological properties of produced monofilaments [16].

In the other study of Melnykowycz et al. [18], a U-shaped CB/SEBS strain sensor was produced. CB and SEBS were mixed in a ratio of 50:50 by using a torque rheometer. The illustration of the sensor can be seen from Figure 2.15 [18].

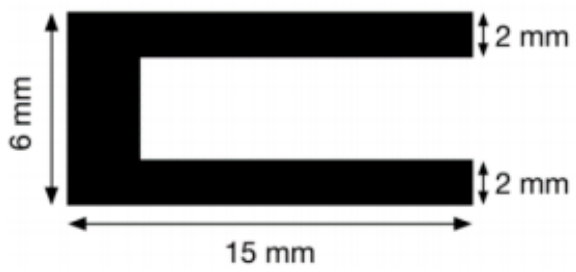

Figure 2.15. The schematic illustration of a U-shaped sensor, consisting of 50 wt% CB/SEBS [18]

In order to observe the piezoresistive behavior, cycling tests were performed. The gauge length was adjusted to 40 mm, while the active length of the sensor was 10 mm (Figure 2.16). As can be seen, electrodes were attached to both ends of the sensor. The mechanical set-up for cycling tests is given in Figure 2.17 [18].

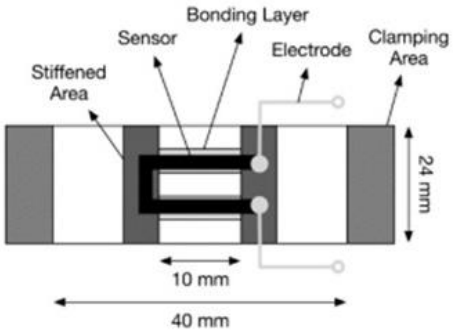

Figure 2.16. The illustration of the sensor for cyclic tests [18]

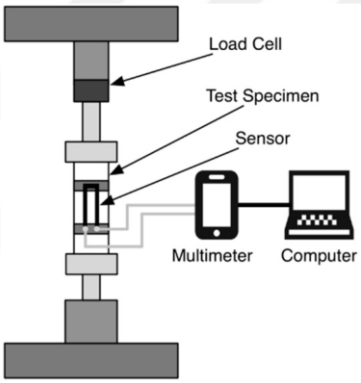

Figure 2.17. The illustration of mechanical test setup for cyclic tests [18]

The strain levels and hold times applied to the sample can be seen from Table 2.3. The results of an initial six different conditions are given in Figure 2.18. The sensor showed positive piezoresistive behavior under different strain levels. With the increasing strain level, resistance change also increased [18].

Table 2.3. Strain ranges for the cyclic tests [18]

Strain Test 1	**10%-5%**	**20%-15%**	**30%-25%**	**40%-35%**	**50%-45%**	**35%-15%**
Hold Time	60 s	60 s	60 s	60 s	60 s	60 s
Strain Test 2	50%-45%	30%-25%				
Hold Time	300 s	300 s				

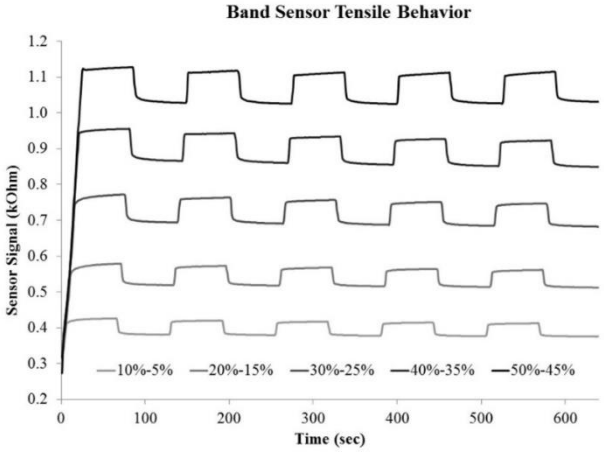

Figure 2.18. The resistance values of the sample under different test conditions [18]

In all strain levels, the resistance change remained almost the same for the first 5 initial cycles (Figure 2.19a). GF was calculated for both maximum and minimum strain levels. It was shown that the highest GF values were obtained under minimum strain levels. The highest GF was obtained under 5% strain (test 10%-5%) [18].

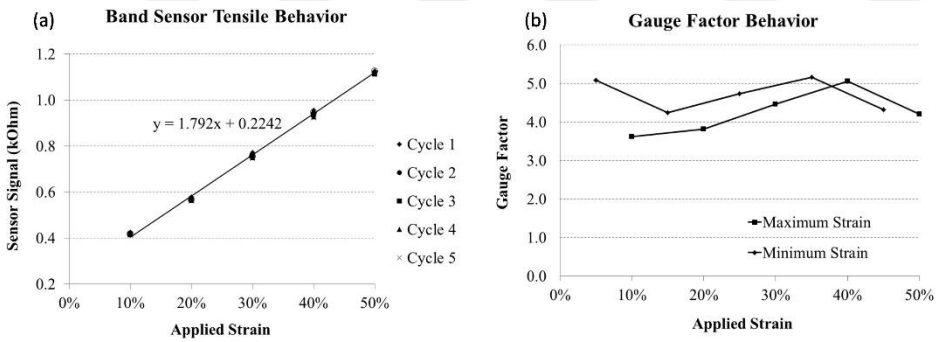

Figure 2.19. Depending on applied strain (a) resistance change, and (b) GF [18]

As a summary of the study, a U-shaped band sensor was fabricated and the working strain range of the sensor was determined between 5-50%. For all conditions, the sensor showed a positive piezoresistive response and high stability. GF was above 3.5 under all test conditions. The band sensor was placed on the wrist for further analysis. The change in pulse was monitorized to calculate the heart rate and the sensor was found successful in terms of health monitoring. The composite with a high amount of CB can be considered as the most important disadvantage in terms of flexibility [18].

Zheng et al. [50] fabricated a piezoresistive strain sensor, consisting of CB and TPU. The ultrasonication method was used to disperse CB particles in TPU/Dimethylformamide (DMF) solution. The production method of the study was designed in order to obtain flocculate with the addition of methanol under high stirring speed. After vacuum filtering and drying of flocculates, compression molding was performed in order to obtain homogenous films. Copper tapes, used as a probe, were adhered to the surface by a silver paint on both ends of the film for electrical and electromechanical analysis (Figure 2.20) [50].

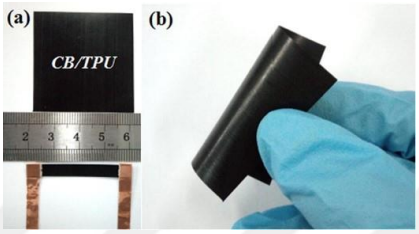

Figure 2.20. (a) Digital images of 10 wt% CB/TPU composite with electrodes and (b) the illustration of the flexibility of 10 wt% CB/TPU composite [50]

Morphology of 8 wt% CB/TPU composite was analyzed by SEM (Figure 2.21). The electrically conductive network of CB was shown clearly from SEM images. It was reported that CB particles were highly dispersed in the matrix by ultrasonication. The particle size of CB was given 30 nm. It was seen that some agglomerations occurred in the composite [50].

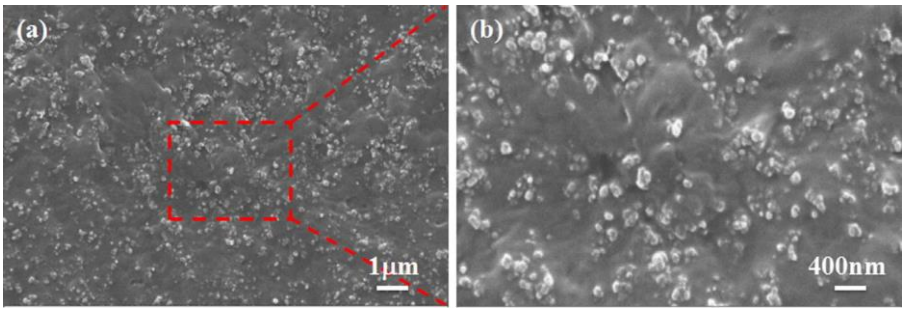

Figure 2.21. (a) and (b) SEM images of 8 wt% CB/TPU composite, scale bar: 1 μm and 400 nm, respectively [50]

Volume resistivity, based on the filler loading, was measured by a digit precision multimeter. It was shown that the electrical conductivity of the composite increased parallel with the higher filler loading. Percolation was obtained between 1-4 wt% CB/TPU (Figure 2.22). It was reported that lower filler content is preferable because TPU composite with high CB particles led to a decrease in flexibility of the composite [50].

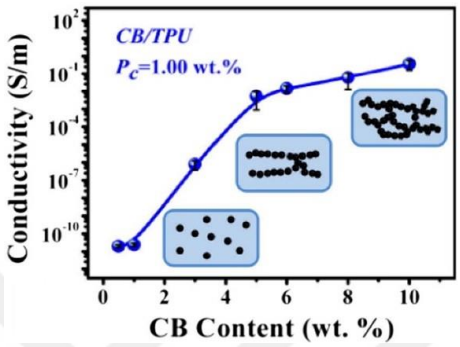

Figure 2.22. Conductivity of TPU samples as a function of CB concentration [50]

Composites with similar electrical conductivity values were used for electromechanical analysis. The relative resistance change against different strain levels was performed, the standard deviation of five samples was calculated and can be seen from Figure 2.23a. It was shown that CB based sensor was used to detect high strain levels, around 90 %. But above 60% strain level, the conductive network started to break down and it resulted in a sharp resistance change. Figure 2.24b shows the change in resistance of the sensor under strain level 0-60 %. With increasing strain levels, the standard deviation of CB-based sensor increased. Up to 20% strain level, the sensor showed an almost linear characteristic, and GF was calculated as 10.8 under %20 deformation [50].

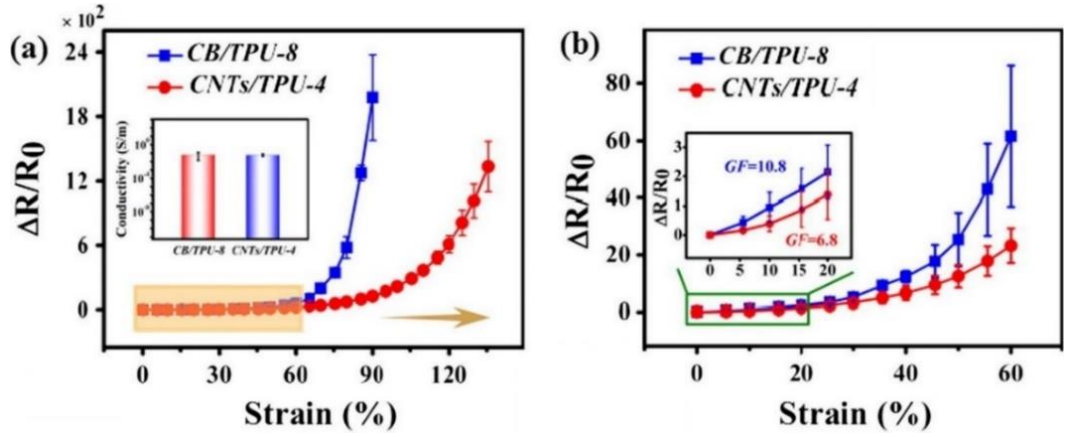

Figure 2.23. (a) Relative resistance of composites under different strain levels up to 120 %, Inset: Electrical conductivity values of the composites chosen for sensor analysis, and (b) Relative resistance of composites up to 60 % strain level, Inset: Resistance change between 0-20 % strain and GF values [50]

The cyclic behavior of the composites was analyzed under 10 and 20% strain levels. Figure 2.24 a shows the resistance change of 8 and 10 wt% CB/TPU sensors for the first ten cycles as a function of 10% strain level. For both filler contents, resistance change increased during loading. For unloading, the resistance change decreased, and then, the slow increase was observed. Similar behavior was observed in the other nine cycles. It was also shown that at high filler concentration, the resistance change was lower. 8wt% CB/TPU sensor was used to analyze the cyclic behavior under 20% strain (Figure 2.24c). When the behavior was compared to the 10% strain level, it can be seen clearly that the resistance change was higher for 20% deformation. Under both deformations, CB-based sensors showed positive piezoresistance [50].

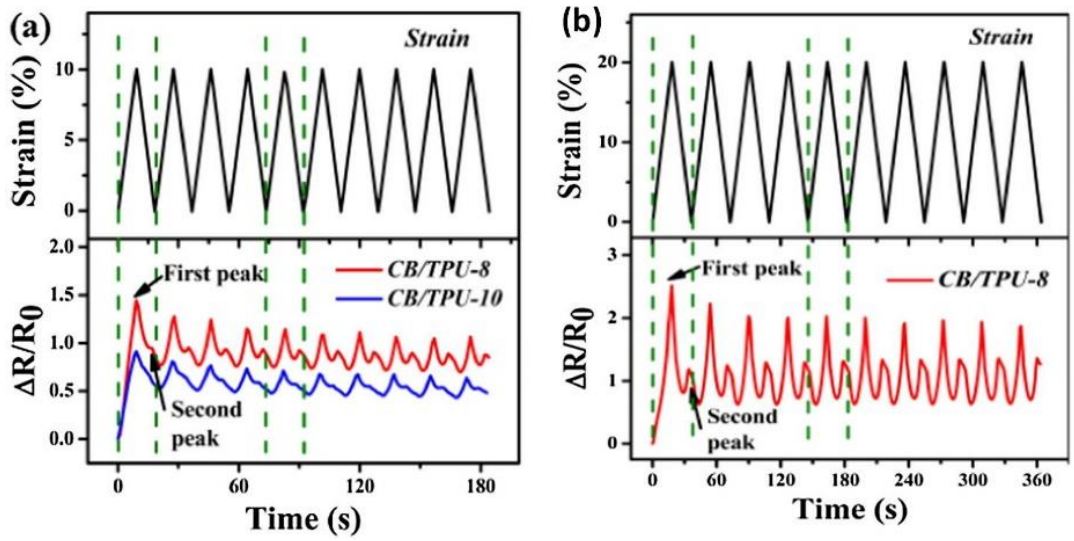

Figure 2.24. Cyclic behavior of CB based sensors under (a) 10, and (b) 20% strain levels [50]

In order to analyze the long-term behavior of the sensors, the cyclic test was performed for 2000 loading-unloading cycles (Figure 2.25). As can be seen from Figure 2.25, CB based sensor showed high stability. When analyzing $\Delta R/R_0$, the change remained the same middle and end of the cyclic test [50].

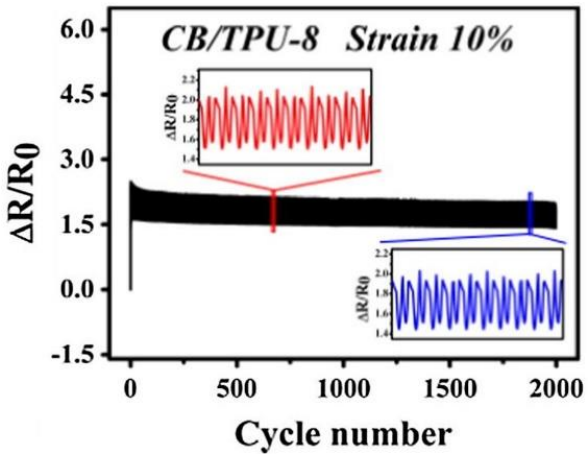

Figure 2.25. The cyclic behavior of 8 wt% CB/TPU sensor under 10% strain level [50]

Initial 100 cycles of different CB loading-based sensor under different strain levels can be seen from Figure 2.26a and c. As in previous analyses, the sensor with lower filler content showed high resistance change and the sensor showed higher sensitivity at high strain levels for the same filler content. In all conditions, CB-based sensors showed stable cyclic behavior [50].

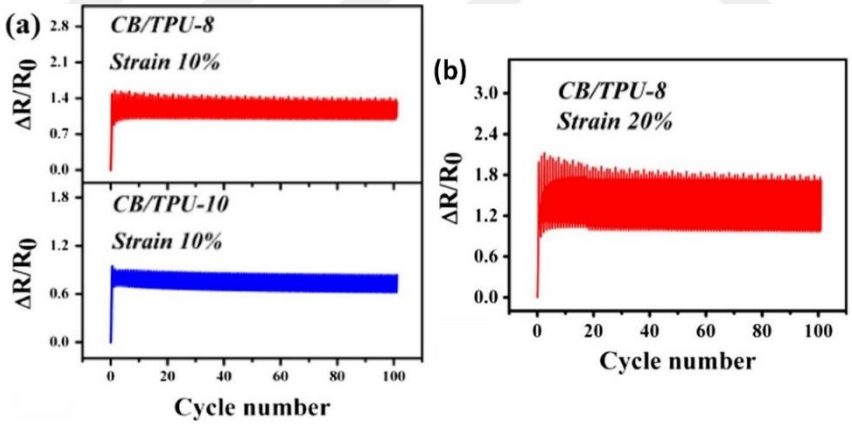

Figure 2.26. (a)The cyclic behavior of 8 and 10wt% CB/TPU sensor under 10% strain level and (b)the cyclic behavior of 8 wt% CB/TPU sensor under 20% strain level [50]

In summary, CB/TPU was prepared by a combination of ultrasonication, flocculation, and compression methods. The morphological, electrical, and electromechanical properties were analyzed. The percolation threshold was determined between 1-4 wt% filler loading. 8 and 10 wt% CB/TPU were chosen for electromechanical analysis. The effect of filler concentration and strain level was also investigated. At higher strain levels, the sensor showed higher sensitivity [50].

Duan et al. [51] fabricated binary and ternary composites by using TPU and/or olefin block copolymer (OBC). As an electrically conducting filler material, CB with the BET surface area of 6.5x10 m^2g^{-1} was used. The effects of annealing treatment on morphological, thermal, mechanical, and piezoresistive properties of the composites were investigated. In the production of binary composites, the matrixes were mixed with 18, 20, 23, and 25 wt% of CB and OBC/CB, and TPU/CB composites were fabricated. On the other hand, for ternary composites, firstly, polymer mixed with filler material (as a mass ratio of 10, 12, and 16), and then the other matrix was added and OBC-CB/TPU, and TPU-CB/OBC composites were produced. In order to fabricate TPU-OBC/CB ternary composite, firstly OB and TPU were blended and CB was added to this blend. The mass ratio of TPU/OBC was kept constant (50/50) for all ternary composites. The annealed samples were represented with "-a" [51].

TEM images of 12 wt% CB filled ternary composites with/without annealing can be seen in Figure 2.27. It was reported that the agglomeration and inhomogeneous dispersion of CB in unannealed composites were observed. After annealing, interfaces between filler and matrixes were improved [51].

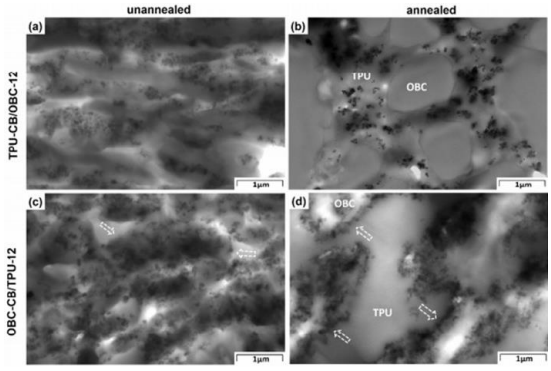

Figure 2.27. TEM images of (a) TPU-CB/OBC-12, (b) TPU-CB/OBC-a-12, (c) OBC-CB/TPU-12, and (d) OBC-CB/TPU-a-12 [51]

Electrical conductivity values of unannealed/annealed binary and ternary composites can be seen in Figure 2.28. Lower percolation was obtained with binary composites. For binary systems, percolation was obtained around 17.5 wt% CB for OBC based composites, while around 18.2 for TPU based composites. In terms of annealing treatment, annealed binary and ternary composites had lower percolation threshold [51].

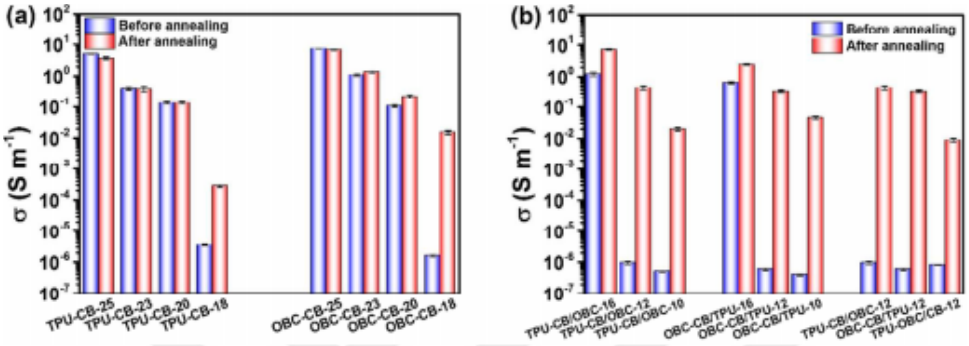

Figure 2.28. Electrical conductivities of (a) binary, and (b) ternary composites before/after annealing [51]

In order to investigate the piezoresistive properties, 20, 23, and 25 wt% CB filled unannealed/annealed binary composites were evaluated at different strain levels (Figure 2.29). It was shown that all sensors could be used under high strain levels. 20 wt% CB filled unannealed composites showed the highest sensitivity for both matrixes. Following these sensors, annealed composites, consisting of 20 wt% CB, showed high sensitivity [51].

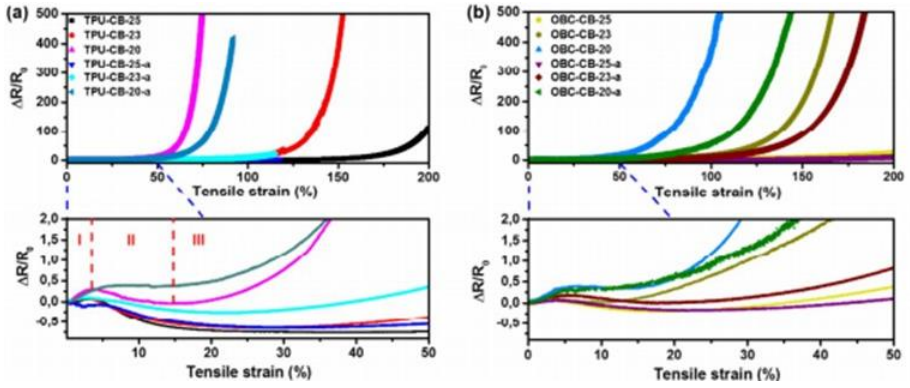

Figure 2.29. Under different strain levels, the resistance change of (a) TPU based binary composites, and (b) OBC based binary composites [51]

For unannealed/annealed ternary sensors, it was shown that annealed samples with low filler content showed higher sensitivity (Figure 2.30a, b, and c). When compared 12 wt% CB annealed ternary samples (TPU-CB/OBC, OBC-CB/TPU, and TPU-OBC/CB), the blend-based sensor showed the highest sensitivity [51].

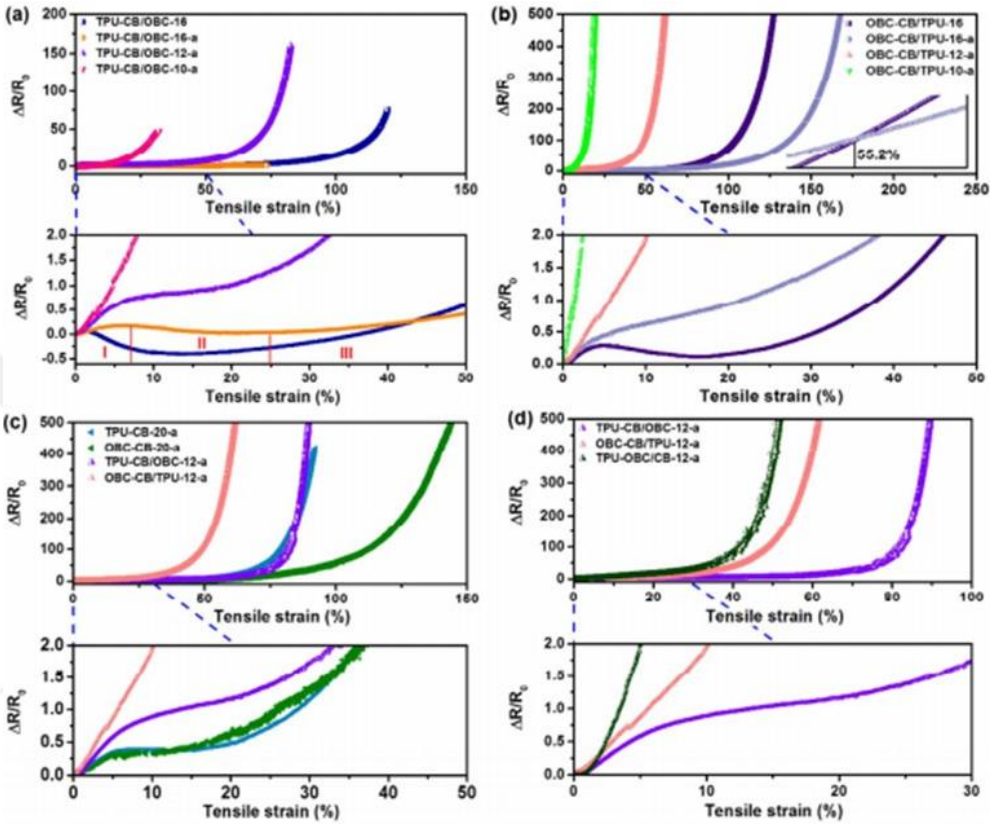

Figure 2.30. Under different strain levels, the resistance change of ternary composites based on (a) TPU-CB/OBC, (b) OBC-CB/TPU (c), and (d) comparison of binary/ternary unannealed/unannealed sensor [51]

In summary, unannealed/annealed binary and ternary samples were fabricated by using different matrixes; TPU and OBC. One of the most important contributions of the study was showing the effect of annealing treatment on the electrical and piezoresistive properties of the sensor. Another contribution of the study was to fabricate binary and ternary composites and their effects on the sensing properties. In the study, it was shown that after annealing, morphological, electrical, and sensing properties of the sensors improved [51].

In another study of Duan et al. [32], binary and ternary composites were fabricated as in their previous study. TPU, OBC, and the blend of the two polymers were used as the matrix. In this study, carbon black particles (CBs) with different surface area values and the mixture of CBs were used (Table 2.4). TPU/OBC ratio changed as 50/50, 60/40, and 30/70. The composites and blends were fabricated by a twin-screw extruder. The % weight ratio of CB in binary and ternary composites varied between 10 and 20; 5 and 12, respectively [32].

Table 2.4. Properties of CBs used in the study [32]

Characteristic	CB_1	CB_2
Average diameter (nm; primary particles)	3.8 x 10	3.0 x 10
DBP[a] adsorption (10^{-2} ml g^{-1})	1.9 x 10^2	4.2 x 10^2
BET[a] surface area (m^2 g^{-1})	6.5 x 10	10^3
Density (g cm^{-3})	1.8	1.3

[a]DBP: Dibutyl phthalate; BET: Brunauer-Emmett-Teller

TEM images of unannealed/annealed ternary composites can be seen in Figure 2.31. Heterogenous dispersion and accumulation in the OBC matrix were observed in the annealed sample. For unannealed composites, filler material dispersed homogeneously and CB preferably dispersed in the TPU phase [32].

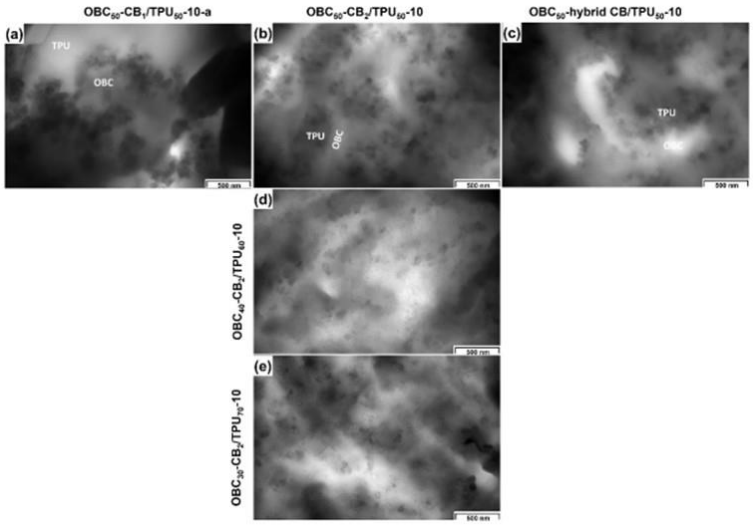

Figure 2.31. TEM images of 10 wt% of CB filled (a) OBC_{50}-CB_1/TPU_{50}-a, (b) OBC_{50}-CB_2/TPU_{50}, (c) OBC_{50}- hybrid CB/TPU_{50}, (d) OBC_{40}-CB_2/TPU_{40}, and (e) OBC_{30}-CB_2/TPU_{70} composites [32]

Before and after annealing treatment, electrical conductivity values of ternary composites can be seen in Figure 2.32. For all compositions, the conductivity of samples was improved with annealing treatment. When the composites were compared, lower percolation threshold was determined for CB_2 filled composites [32].

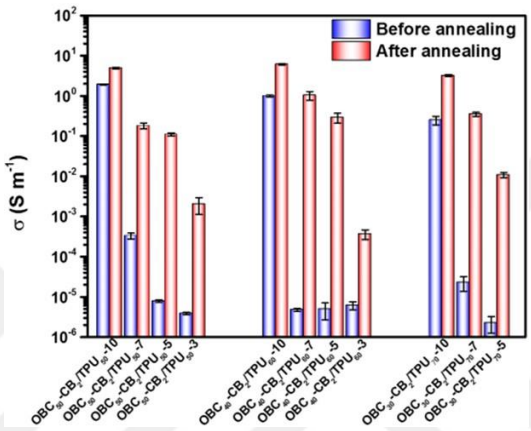

Figure 2.32. Electrical conductivities of ternary composites before/after annealing [32]

Resistance change under different strain levels can be seen in Figure 2.33. In Figure 2.33a, the effect of filler concentration on piezoresistive properties of TPU based composites was investigated. For all concentrations, the sensors showed a nonlinear behavior and with the increasing strain level, exponential behavior was observed. In Figure 2.33b, the effect of polymer concentration was also examined. It was shown that TPU based binary composites showed sharper increase compared with OBC based samples at the same filler concentration. The effect of annealing treatment can be seen in Figure 2.33c. It was concluded that similar behavior was obtained at high filler concentration while unstable behavior was observed at low CB content. The resistance change as a function of the surface area of filler material can be seen in Figure 2.33d. A rapid increase in resistance was observed with the composites filled with high surface area CB_2 [32].

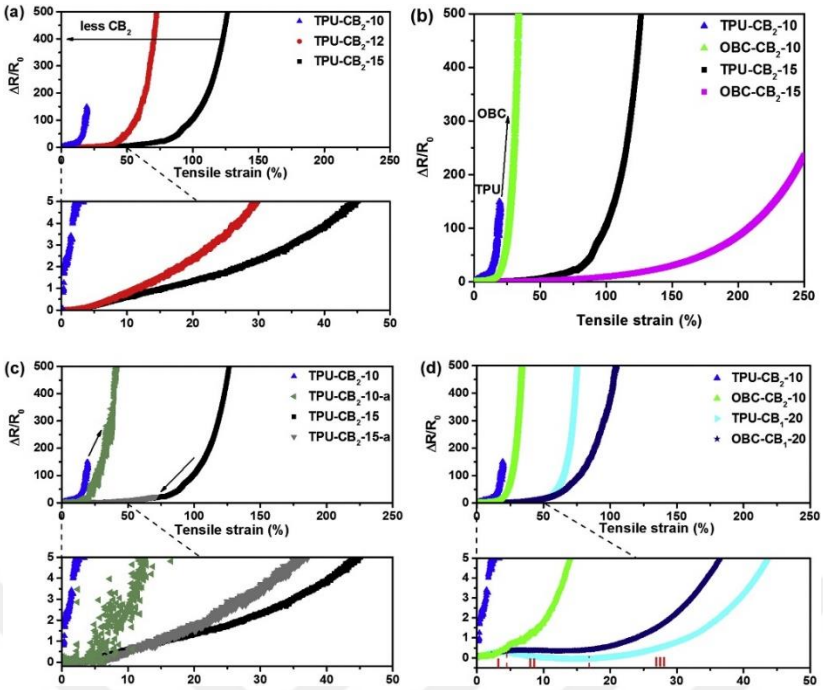

Figure 2.33. Under different strain levels, the resistance change of (a) TPU based binary composites; comparison of (b) matrix type, (c) annealing treatment, and (d) carbon black type [32]

Effect of annealing, filler concentration, blend ratio, and filler type of piezoresistive behavior at different strain levels can be seen in Figure 2.34. In Figure 2.34a, the annealed sample showed higher resistance change. Annealed samples with different ratios had a similar behavior up to 5% strain and the sensor, consisting of the lowest filler ratio, showed the highest resistance change under 5% strain. In terms of blend ratio, composites, having the highest ratio of TPU, showed the highest sensitivity. When the effect of CB type was examined, the sensitivity can be given as annealed composite, consisting of lower surface area CB > hybrid sample > unannealed composite filled with the high surface area of CB [32].

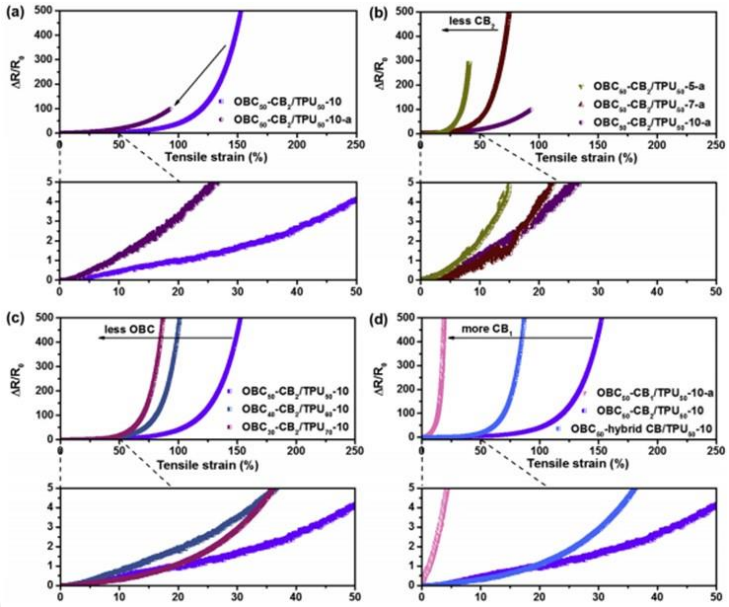

Figure 2.34. Under different strain levels, the resistance change of ternary composites and compo (a) TPU based binary composites; comparison of (b) matrix type, (c) annealing treatment, and (d) carbon black type [32]

As a summary of the study, the effects of annealing treatment, CB type, polymer type, and blend ratio on thermal, morphological, mechanical, piezoresistive properties were investigated. One of the contributions of the study was to compare the effect of filler type and hybrid fillers on sensing properties. Another contribution of the study was to produce binary and ternary composites with different polymer matrixes [32].

Poudel et al. [20] studied the effect of the production method on thermal, mechanical, morphological, and piezoresistive properties. SEBS with the S/EB ratio of 29/71 and 1, 5, and 10 wt% CB filled composites were prepared. Sensors were fabricated with and without supercritical fluid (SCF) assisted extrusion. Digital images of composite and sensor, attached with gold electrodes, can be seen from Figure 2.35 [20].

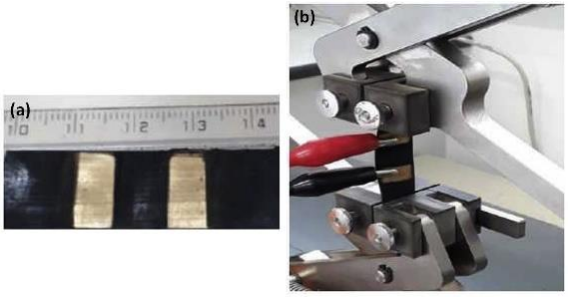

Figure 2.35. (a) Digital images of the composite, and (b) sensor set-up [20]

Morphology of 1 wt% CB/SEBS composites can be seen from Figure 2.36. Composites produced by SCF-assisted extrusion showed better dispersion. Agglomerations could be seen composites were fabricated without the SCF method [20].

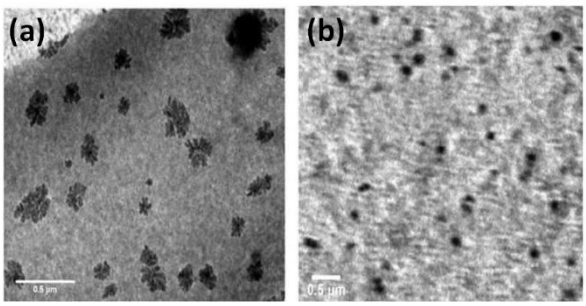

Figure 2.36. TEM images of 1 wt% CB filled composites, produced (a) without SCF, and (b) with SCF [20]

Percolation region was observed around 5 and 10 wt% of filler loading for composites with SCF and without SCF, respectively. In order to analyze cyclic properties under 5% strain, 10 wt% CB filled composites were chosen for both production methods. Irregular changes were obtained for the composites produced without SCF. A decreasing trend was observed for SCF-assisted sensor (Figure 2.37) [20].

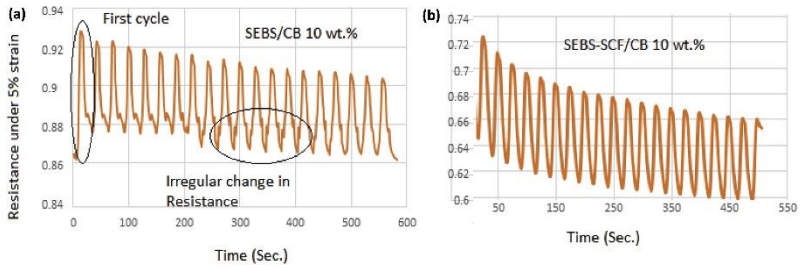

Figure 2.37. Cyclic behavior of the composites, fabricated (a) without SCF, and (b) with SCF at 5% strain [20]

GF was calculated at 2% strain for SCF-assisted 5 and 10 wt% CB/SEBS and 10 wt% CB/SEBS without SCF (Figure 2.38a). The highest GF was obtained as around 9 for SCF-assisted 5 wt% CB/SEBS. Higher GF values were calculated for the same sensor at different strain levels (Figure 2.38b) [20].

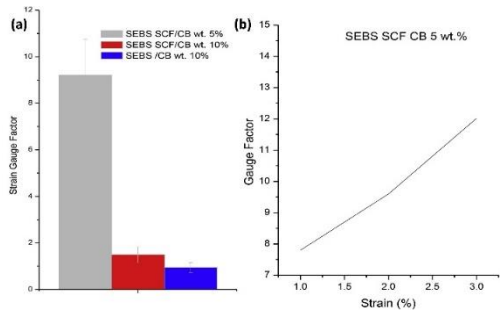

Figure 2.38. (a) GF of sensors at 2% strain, and (b) GF of SCF-assisted 5 wt% CB/SEBS sensor at different strain levels [20]

As a summary, Poudel et al. investigated the effects of the fabrication method on the electrical and electromechanical properties of the CB/SEBS composites. The study was useful in terms of using and understanding the effects of supercritical fluid on composite properties. Better dispersion and lower percolation were obtained by the SCF method. Under the same strain level, higher GF values were obtained for SCF-assisted samples. With the increasing strain level, higher GF values were obtained for 5 wt% CB/SEBS-SCF assisted composite [20].

2.3.2 Piezoresistive strain sensors with carbon nanofiber filled thermoplastic elastomer

The study about investigating piezoresistive strain sensing properties of carbon nanofiber filled thermoplastic elastomer is very limited. The one study carried out by Turgut et al. [21]. SEBS gels and neat SEBS based sensors were produced. Vapor grown carbon nanofiber (VGCNF) was used as an electrically conducting material and to obtain a good dispersion, filler material and matrix were mixed by using a high shear mixer. Homogenously dispersion of fillers for both matrixes was confirmed by SEM images (Figure 2.39 and 2.40) [21].

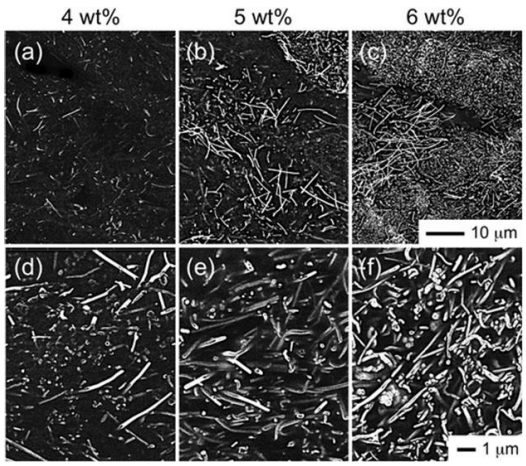

Figure 2.39. SEM images of SEBS gel, consisting of (a), (d) 4 wt%, (b), (e) 5 wt%, and (c), (f) 6 wt% VGCNF [21]

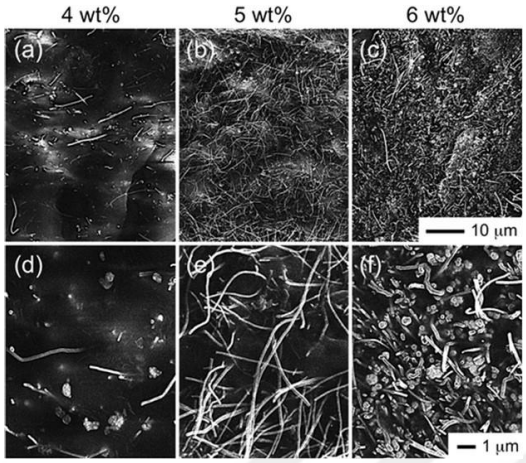

Figure 2.40. SEM images of neat SEBS, consisting of (a), (d) 4 wt%, (b), (e) 5 wt%, and (c), (f) 6 wt% VGCNF [21]

In order to analyze the volume resistivity of composites, filler loading was varied between 1-7 wt% (Figure 2.41). Percolation region for both composites was obtained between 2-3 wt% VGCNF. It was shown that neat SEBS had lower volume resistivity value [21].

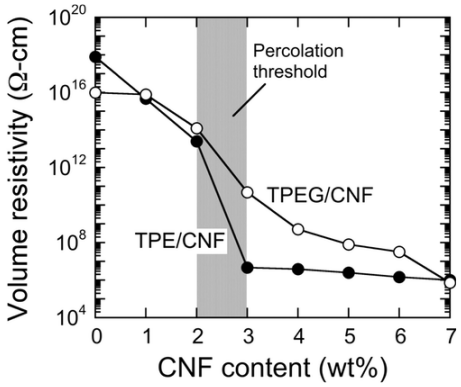

Figure 2.41. Volume resistivity of composites depending on filler loading [21]

The cyclic behavior of the sensors was evaluated at 20% strain with a test speed of 20 and 100 mm/min (Figure 2.42 and 2.43). For all conditions, VGCNF filled sensor with neat SEBS matrix showed higher sensitivity and stability compared to SEBS gel sensor. Both sensors had a negative piezoresistive behavior [21].

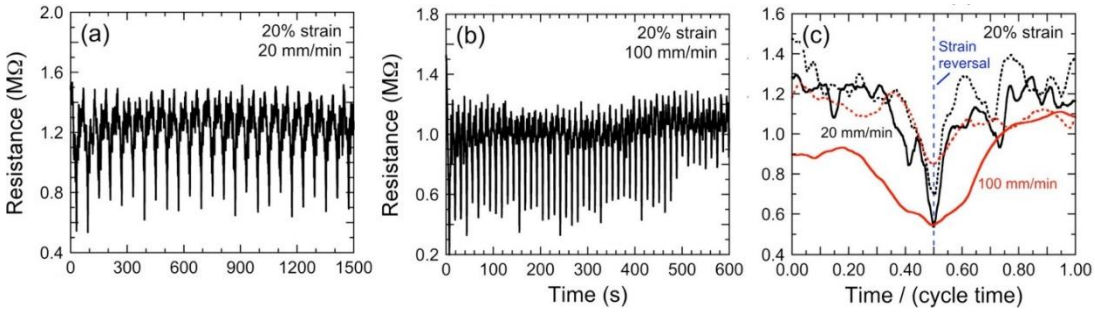

Figure 2.42. Cyclic behavior of SEBS gel sensor at 20% strain level and different test speed (a) 20 and (b) 100 mm/min, (c) resistance vs normalized time graph at 20% strain for both test speeds [21]

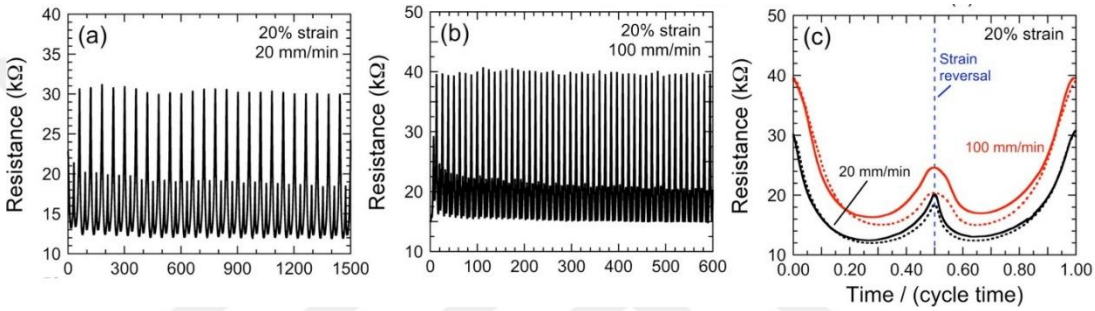

Figure 2.43. Cyclic behavior of SEBS sensor at 20% strain level and different test speed (a) 20 and (b) 100 mm/min, (c) resistance vs normalized time graph at 20% strain for both test speeds [21]

In summary, Turgut et al. fabricated strain sensors with two different matrixes, SEBS gel, and neat SEBS. VGCNFs were dispersed homogeneously by using a high shear mixer. Percolation region was observed between 2-3 wt% filler loading for both composites. The difference of matrix showed an important effect on the cyclic behavior of the sensors. The most important contribution of the study was to explain negative piezoresistance. Both sensors showed a negative piezoresistive behavior at all strain levels and test speeds. Another useful contribution was to show the effect of polymer matrix type (gel or neat polymer) on sensing properties [21].

3. MATERIALS AND METHODS

3.1 Materials

In the study, two different SEBS were used, regarding their styrene to ethylene-butylene (S/EB) ratio. SEBS, Kraton G1657, and G1643 with S/EB ratio of 13/87 and 19/81 and melt flow index of 8 g/10 min and 75 g/10 min (under 5 kg load at 200 ˚C), respectively. SEBS with lower styrene content referred as SEBS-M, while SEBS-S with higher styrene content referred as SEBS-S. Two different conducting filler materials were used. Carbon black (CB), BET surface area of 62 m^2/g, and the particle size of 30-50 nm, was bought from MTI, (Timical Super C65). Vapor-grown carbon nanofiber (VGCNF) had an average fiber diameter of 130 nm and length was between 20 to 200 μm (Sigma Aldrich). Toluene (Merck) was used as a solvent. The fabric used for the textile sensor contained 75% polyamide and 25% elastane and was kindly supplied from a local medical store.

3.2 Methods

3.2.1 Preparation of the nanocomposites

Nanocomposite films were prepared in five steps (Figure 3.1). Firstly, by adding toluene with the ratio of SEBS:toluene, w:w = 1:4, polymer solution was prepared by a magnetic stirrer for 12 h (Wisd, 700 rpm). Secondly, fillers were dispersed with 5 g of toluene by using a high-shear planetary mixer (Kurabo Mazerustar KK 250) under 1500 rpm for 90 s. Thirdly, the polymer solution was added into a filler-solvent mixture and mixed by the high-shear planetary mixer. Then, the polymer-filler suspension was poured into the petri dish and at 40 °C, the solvent casted samples dried in an oven to remove the solvent. In the fifth step, under 3 MPa, films were obtained by compression molding at 180 °C for 1 min. The thickness of all nanocomposite films was measured by thickness meter (Asimeto) and the average value was around 400-500 μm. The properties of the nanocomposite films consisting of CB, VGCNF, and CB-VGCNF at various concentrations were given with details in Table 3.1.

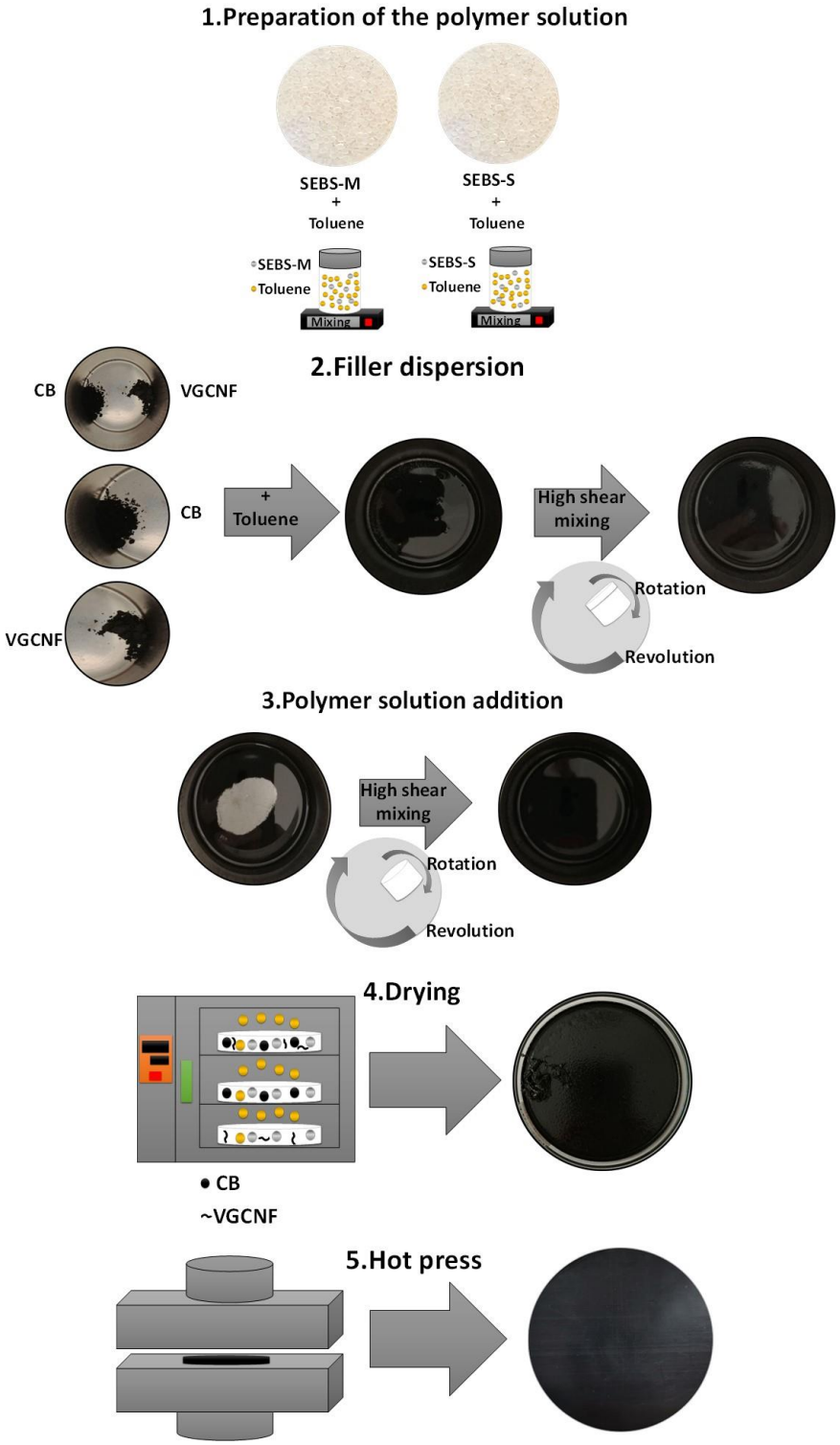

Figure 3.1. Preparation of CB, VGCNF, and CB-VGCNF filled SEBS-M/S samples [26]

Table 3.1. The composition of the SEBS-M and SEBS-S based nanocomposite films [26]

SEBS-M	**Filler Type and Concentration (wt%)**		**SEBS-S**	**Filler Type and Concentration (wt%)**	
Code	CB	VGCNF	Code	CB	VGCNF
1	0	0	20	0	0
2	0.25	0.25	21	0.25	0.25
3	0.5	0.5	22	0.5	0.5
4	0.75	0.75	23	0.75	0.75
5	1.75	1.75	24	1.75	1.75
6	2.5	2.5	25	2.5	2.5
7	3.25	3.25	26	3.25	3.25
8	0.5	-	27	0.5	-
9	1	-	28	1	-
10	1.5	-	29	1.5	-
11	3.5	-	30	3.5	-
12	5	-	31	5	-
13	6.5	-	32	6.5	-
14	-	0.5	33	-	0.5
15	-	1	34	-	1
16	-	1.5	35	-	1.5
17	-	3.5	36	-	3.5
18	-	5	37	-	5
19	-	6.5	38	-	6.5

3.2.2 Preparation of the sensors

Nanocomposites tested as strain sensors can be seen from Table 3.2. In order to determine the piezoresistive behavior, nanocomposite films were cut (25 mm × 80 mm, width x length). Four Cu leads were placed on the 50 mm length of the film and the distance between the leads were 10 mm (Figure 3.2). Solvent-based glue, consisting of 40 wt% CB, was used to mount the Cu leads on the nanocomposites (Figure 3.3). After that, samples were placed between the grips of the mechanical characterization system, and the Cu leads of the samples were connected to the electrical characterization system (current source and voltmeter). The tests were performed under 5, 10, and 20% strain and 5 and 50 mm/min. Since the best results were obtained under 20% strain with a test speed of 5 mm/min, only these results were given for all samples.

Table 3.2. The composition of the samples used as a strain sensor [26]

SEBS-M	**Filler Type and Concentration (wt%)**		**SEBS-S**	**Filler Type and Concentration (wt%)**	
Sample Code	CB	VGCNF	**Sample Code**	CB	VGCNF
6	2.5	2.5	**24**	1.75	1.75
7	3.25	3.25	**25**	2.5	2.5
12	5	-	**26**	3.25	3.25
13	6.5	-	**31**	5	-
18	-	5	**32**	6.5	-
19	-	6.5	**37**	-	5
-	-	-	**38**	-	6.5

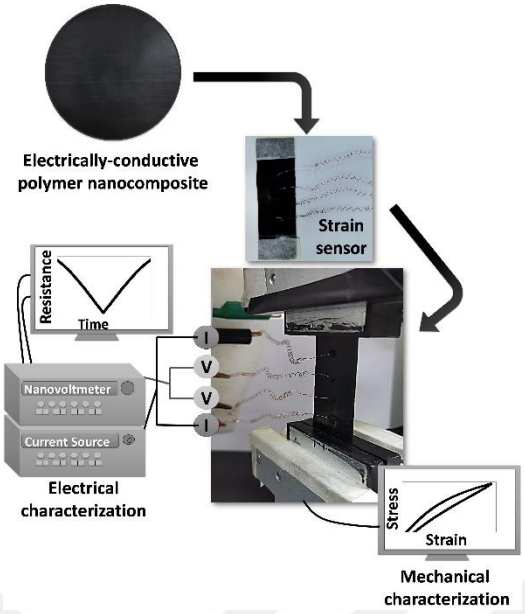

Figure 3.2. Preparation of the strain sensors and illustration of electrical and mechanical characterization systems [26]

3.2.3 Preparation of the fabric sensors

Fabric (75% polyamide and 25% elastane) was cut in the size of 35 mm × 85 mm (width x length) (Figure 3.3). The composite solution was coated on the 25 mm x 80 mm of the fabric by a coating blade. After drying, four Cu leads were mounted on the fabric sensor as described in the electromechanical characterization of nanocomposites. Then, the fabric sensor was located between the grips of the mechanical characterization system and piezoresistive behavior was monitored. The tests were performed under 5, 10, 20, and 25% strain with the test speeds of 5 and 50 mm/min. Since the best results were obtained under 20% strain with a test speed of 5 mm/min, only that results were given for 4 wt% hybrid filler filled fabric sensor.

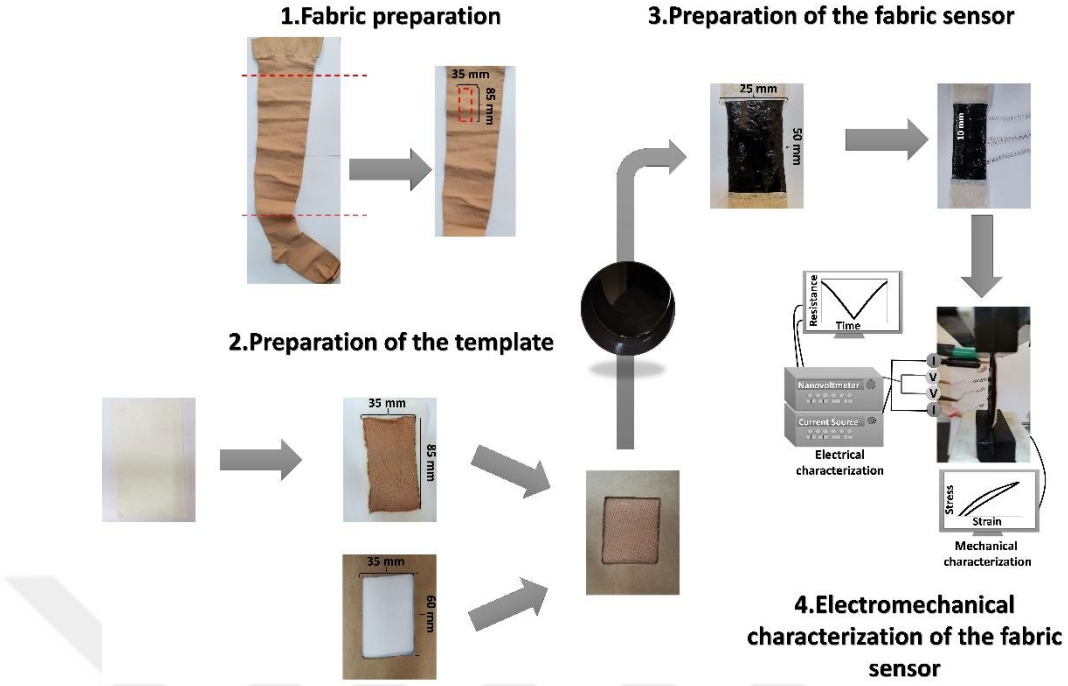

Figure 3.3. Preparation of the textile based hybrid strain sensors

3.2.4 Characterization

The morphology analysis of CB, VGCNF, CB-VGCNF based nanocomposites, and fabric sensor were carried out by Field Emission Scanning Electron Microscope (FESEM, JEOL JSM-6400) at Middle East Technical University (30 kV). Before morphological analysis, samples were sputter-coated with a thickness of 3-6 nm with gold-palladium alloy.

In order to determine the percolation behavior of the nanocomposite films, the volume resistivity was measured according to the ASTM D257 standard. The thickness of the nanocomposite films was measured by a thickness meter (Asimeto). At least 5 measurements were conducted by using Electrometer (6517B Keithley) and a resistivity chamber (8009 Keithley) and the average values and standard deviation were calculated.

Mechanical characterization was carried out by Devotrans DVT universal load frame. The nanocomposite films were cut to the size of 5 mm × 15 mm (width x length) and the test speed was 100 mm/min. The thickness of the specimens was measured by using the Asimeto digital thickness meter. At least three analyses were performed and average values and standard deviation values were calculated.

In order to analyze the piezoresistive properties of the sensors, a load frame (Devotrans DVT), a current source (Keithley 6221), and a nanovoltmeter (Keithley 2182A) were used. For mechanical analysis, sensors were placed between the load frame. The distance between the grips was 50 mm. The tests were carried out uniaxially and dynamically under different test speeds (5, 50 mm/min) and different strain levels ((5, 10, 20 %). Since the best results were obtained under 20% strain with a test speed of 5 mm/min, only these results were given for all samples. Electrical analysis was performed simultaneously with the mechanical cycling according to the four-probe measurement method.

4. RESULTS

4.1 CB/SEBS Piezoresistive Strain Sensors

4.1.1 Morphological characterization

Before the morphological characterization, samples were sputter-coated with 3-6-nm thick Au/Pd alloy, and cross-sectional images of nanocomposites that were chosen considering their electrical conductivity were captured by FESEM. For SEBS-M (Figure 4.1a), 0.5 (insulation region), 5 (percolation region), and 6.5 (saturation region) wt% CB-based samples were analyzed. The 0.5 (insulation region), 3.5 (percolation region), and 6.5 (saturation region) wt% CB-filled SEBS-S samples were chosen for morphological analysis (Figure 4.1b). In all composites, dark grey parts represent the electrically insulating polymer matrix, while light grey shows the electrically conducting filler material. As can be seen from the images, CB particles had a spherical structure and were well-dispersed in both SEBS matrixes for all concentrations. A good filler-matrix interface was obtained regardless of polymer type. At low filler loadings, CB particles were highly separated and the conductive network didn’t form. With the increase of concentration, the distance between filler particles decreased, and the conductive network was obtained at percolation and saturation regions [26].

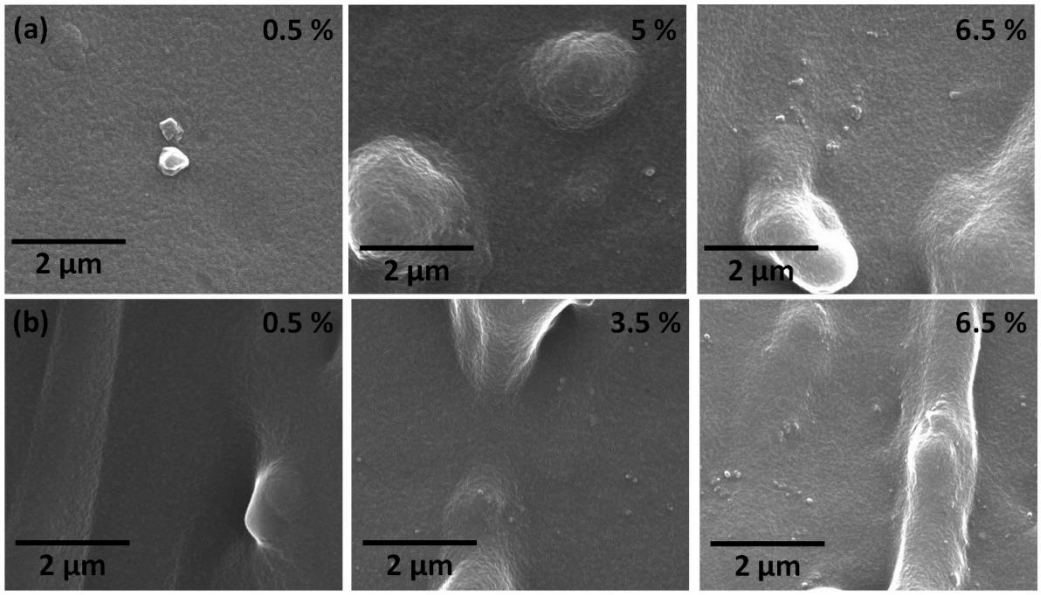

Figure 4.1. FESEM images of (a) CB/SEBS-M and (b) CB/SEBS-S [26]

4.1.2 Electrical characterization

By measuring the volume resistivity of samples, the percolation graphs of CB-filled SEBS-M and SEBS-S nanocomposites were obtained as a function of filler loading (Figure 4.2). The normalized volume resistivity values were given in Table 4.1. CB content was varied between 0-6.5 wt% for both SEBS. With the increase in filler content, volume resistivity values were decreased. The three distinct regions were observed with the addition of filler. The regions were called; insulation, percolation, and saturation. For SEBS-M composites, the regions were determined as 0-3.5, 3.5-5, and 5-6.5 wt% CB loading. On the other hand, for SEBS-S based nanocomposites, insulation, percolation, and saturation regions were obtained as 0-1.5, 1.5-5, and 5-6.5 wt% CB, respectively. For both polymer matrixes, in the insulation region, the significant change in volume resistivity didn't observe and the conductive network didn't form (Figure 4.1). As can be seen from ρ_0/ρ ratios in Table 4.1. 0-3.5 wt% CB filled SEBS-M and 0-1.5 wt% CB filled SEBS-S nanocomposites had almost the same orders of magnitude. The percolation threshold was determined between 3.5-5 and 1.5-5 wt% CB for SEBS-M and SEBS-S, and the decrease in normalized volume resistivity was nine and seven orders of magnitude, respectively. For both polymer matrixes, a drastic change in volume resistivity wasn't observed between 5-6.5 wt% filler concentration, and the region called saturation. The decrease in ρ_0/ρ ratios was almost the same when the filler loading was increased from 5 wt% to 6.5 wt% CB (Table 4.1).

In terms of the matrix type, the lower percolation was obtained by SEBS-S, and it was probably caused by the difference in the S/EB ratio of two polymers. In the literature, it was reported that conductive fillers were preferably dispersed in the EB phase [52]. By SEBS-S, with a higher S content (higher rigid groups), CB particles had been forced to form a conductive network at lower filler loading. It was concluded that the block size of the polymer matrix is an important criteria for CB-filled samples in terms of electrical conductivity.

Table 4.1. Volume resistivity and ρ_0/ρ values of both SEBS as a function of CB [26]

Filler Concentration (wt%)	**Volume Resistivity (ρ) (ohm.cm)**		**ρ_0/ρ (ohm.cm)/(ohm.cm)**	
	SEBS-M	**SEBS-S**	**SEBS-M**	**SEBS-S**
0	1.09E+17	4.25E+17	1.00E+00	1.00E+00
0.5	2.89E+16	4.69E+16	3.77E+00	9.06E+00
1	1.94E+16	2.98E+16	5.62E+00	1.43E+01
1.5	1.02E+16	1.75E+16	1.07E+01	2.43E+01
3.5	9.01E+15	2.36E+09	1.21E+01	1.80E+08
5	1.97E+07	7.99E+06	5.53E+09	5.32E+10
6.5	9.26E+05	6.55E+05	1.18E+11	6.49E+11

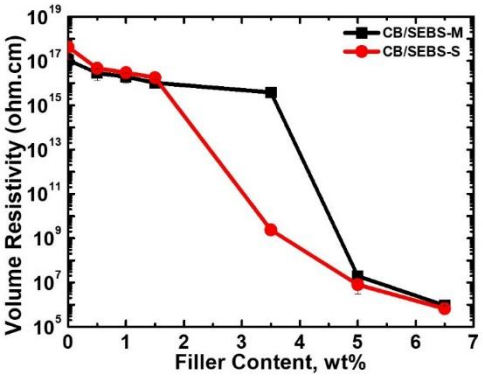

Figure 4.2. Percolation graph of CB filled composites [26]

4.1.3 Mechanical characterization

Mechanical characterization has importance for obtaining information about morphology and determining the limits of materials. The test speed was adjusted to 100 mm/min and at least 3 samples were tested for each group. Traditional stress-strain behavior of thermoplastic elastomer was observed for all CB-filled nanocomposites (Figure 4.3). Average tensile strength, elastic modulus, and tensile strain values of CB-based nanocomposites were given in Table 4.2. Both polymers showed high tensile strain more than 700%. Nanocomposites consisting of SEBS with a higher S content showed higher tensile strain up to 1250%. With the addition of CB up to 5wt% into both SEBS matrixes, the tensile strain of nanocomposites increased and then decreased. For 6.5 wt% CB filled nanocomposites, the tensile strain is still higher than neat SEBS matrixes. The graph about tensile strength and elastic modulus of SEBS-M and SEBS-S as a function of CB loading was given in Figure 4.4. It can be seen that SEBS-M and SEBS-S showed a similar trend with the addition of carbon black. The difference resulted from polymer matrixes with different block sizes. As mentioned before, CB particles were dispersed more homogenously in the matrix with a high EB content. For this reason, it showed higher values, compared to SEBS-S [52].

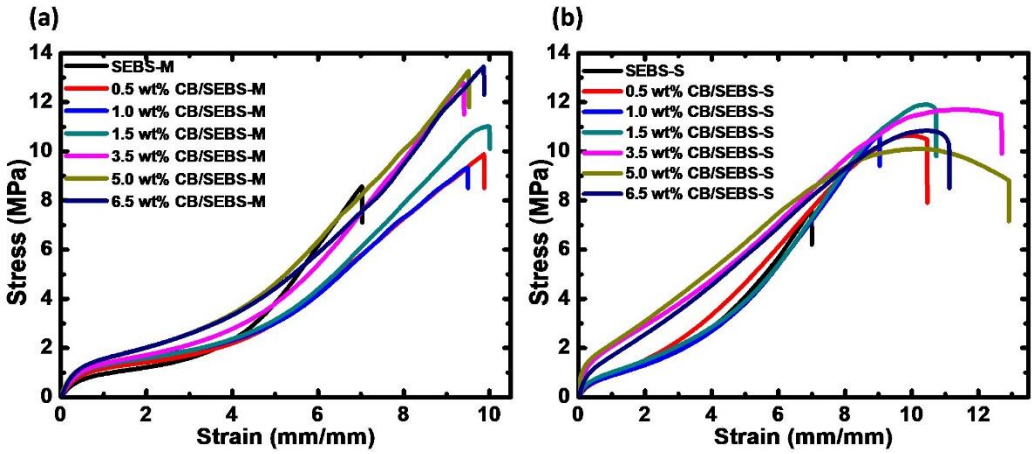

Figure 4.3. Stress-strain curves of (a) CB/SEBS-M and (b) CB /SEBS-S [26]

Table 4.2. Average tensile strength, elastic modulus, and tensile strain values of CB based nanocomposites (SD: Standart Deviation) [26]

Sample	Tensile Strength (MPa)	Normalized Tensile Strength (σ/σ_{SEBS})	Elastic Modulus (MPa)	Normalized Elastic Modulus (E/E_{SEBS})	Tensile Strain (%)	Normalized Tensile Strain ($\varepsilon/\varepsilon_{SEBS}$)
SEBS-M						
SEBS-M	7.50	1.00	2.12	1.00	735.11	1.00
0.5 wt% CB	8.95	1.19	2.31	1.09	947.48	1.29
1.0 wt% CB	10.09	1.35	2.54	1.20	969.34	1.32
1.5 wt% CB	11.43	1.52	2.57	1.21	967.42	1.32
3.5 wt% CB	13.32	1.78	2.68	1.26	956.72	1.30
5.0 wt% CB	12.67	1.69	3.20	1.51	1005.27	1.37
6.5 wt% CB	9.41	1.25	3.34	1.58	824.53	1.12
SEBS-S						
SEBS-S	7.66	1.00	1.71	1.00	735.55	1.00
0.5 wt% CB	10.51	1.37	2.20	1.29	1059.13	1.44
1.0 wt% CB	10.48	1.37	2.28	1.33	1074.51	1.46
1.5 wt% CB	11.94	1.56	2.35	1.37	1009.82	1.37
3.5 wt% CB	11.44	1.49	2.37	1.39	1168.97	1.59
5.0 wt% CB	10.72	1.40	2.65	1.55	1205.60	1.64
6.5 wt% CB	10.29	1.34	2.77	1.62	1012.94	1.38

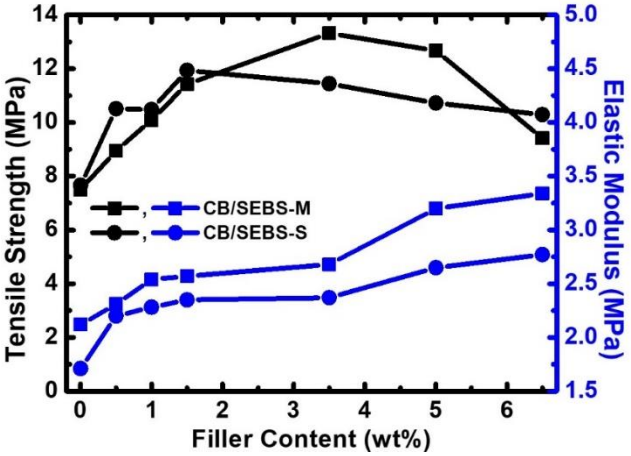

Figure 4.4. Tensile strength and elastic modulus of SEBS-M and SEBS-S as a function of CB loading [26]

4.1.4 Electromechanical characterization

In order to analyze the electromechanical properties, 5 and 6.5 wt% filler filled composites were chosen. In terms of electrical properties, 5 and 6.5 wt% CB/SEBS-M and CB/SEBS-S were determined from saturation regions of the percolation graphs. In order the characterize the sensing properties of composites as a function of filler concentration and polymer matrix, the test speed was adjusted to 5 mm/min, strain rate was 20%, and 50 cycles were performed for all samples. Figure 4.5 showed the test results of 5 and 6.5 wt% CB/SEBS-M and CB/SEBS-S samples for 50 cycles (Figure 4.5a) and initial 5 cycles (Figure 4.5b). Normalized resistance values can be shown depending on the cycle count. In terms of cyclic stability, all sensors were stable. In detail, SEBS with high EB content showed higher stability. SEBS-S based sensor showed stability after the 10th cycle. The noisiness of the cycles can be seen clearly from Figure 4.5b and 5 wt% CB/SEBS-M had a noisy response under given conditions. In terms of sensitivity, sensors, consisting of higher S content of polymer matrix had higher normalized resistance values. With the addition of filler, the sensitivity was decreased for both polymers and it was related to the density of the conductive network in the structure. It can be said that a denser network could lead to lower normalized resistance values. The GF values of the samples depending on cycle count were given in Figure 4.6 and the highest sensitivity was shown sensor with 5 wt% CB-SEBS-S.

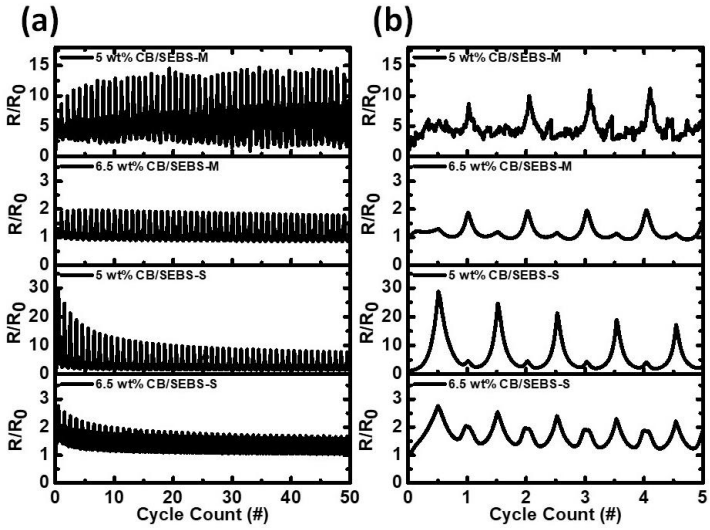

Figure 4.5. Normalized resistance values of 5 and 6.5 wt% CB/SEBS and SEBS-S based on cycle count (a) 50 cycles, and (b) first 10 cycles [26]

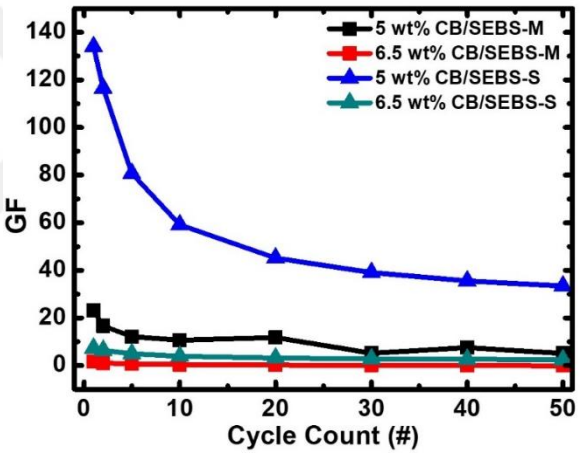

Figure 4.6. GF values of 5 and 6.5 wt% CB/SEBS and SEBS-S samples [26]

4.2 VGCNF/SEBS Piezoresistive Strain Sensors

4.2.1 Morphological characterization

In order to understand dispersion of fibrous filler material and interface between filler and matrix, morphological images of nanocomposites were analyzed by FESEM. The cross-sectional samples were sputter-coated before the characterization. The samples were chosen depending on their electrical properties. The images of SEBS-M and SEBS-S depending on the filler concentration can be seen in Figure 4.7a and Figure 4.7b, respectively. For both SEBS, 0.5 (insulation region), 1.5 (percolation region), and 6.5 (saturation region) wt% VGCNF based samples were analyzed. In Figure 4.7a

and 4.7b, dark grey parts show the electrically insulating SEBS matrix, and light grey parts represent the VGCNFs. The fibrous filler material didn't show a dominant orientation. A good dispersion and filler-matrix interface were observed for all filler concentrations and both matrix types. It was also shown that in the analyzed area, more fillers were observed parallel with the filler concentration. At higher concentrations, the conductive network can be seen easily.

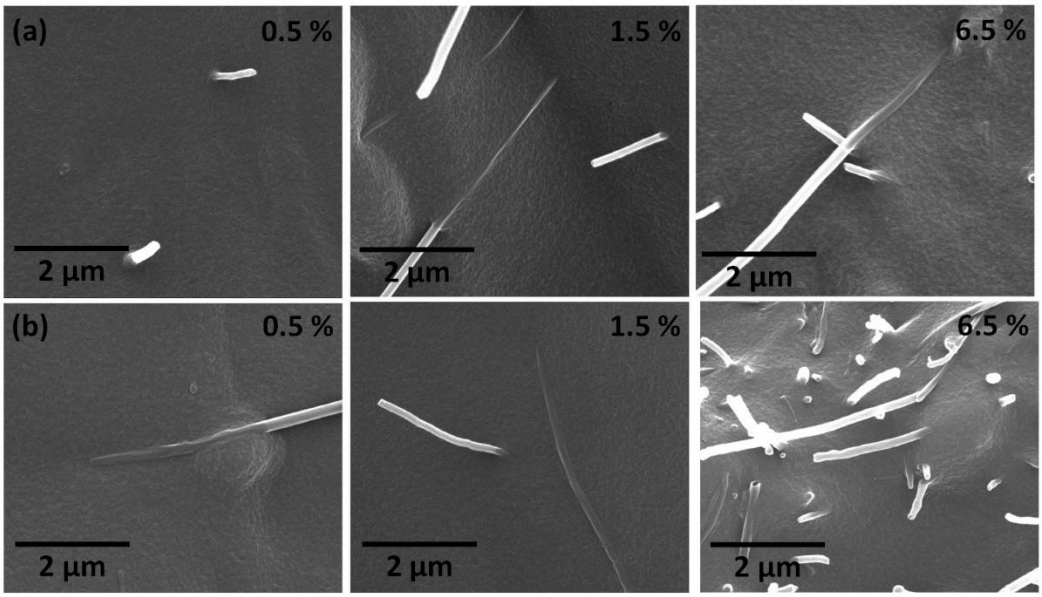

Figure 4.7. FESEM images of (a) VGCNF/SEBS-M and (b) VGCNF /SEBS-S [26]

4.2.2 Electrical characterization

In order to analyze the electrical properties of VGNCF filled SEBS-M and SEBS-S nanocomposites, the volume resistivity was measured as a function of filler loading, which was varied from 0 to 6.5 wt%. The percolation graph and normalized volume resistivity are given in Figure 4.8 and Table 4.3. The expected percolation response was observed for two polymers. The insulating region was determined 0-1.0 wt% VGCNF loading. In this region, the plateau was observed and ρ_0/ρ was almost the same with neat SEBS-M and SEBS-S (Table 4.3). Percolation threshold was obtained between 1-1.5 wt% filled nanocomposites. The decrease in ρ_0/ρ ratio was eight and nine orders of magnitude for SEBS-M and SEBS-S, respectively. At higher concentrations, drastic change in volume resistivity was not observed and filler loading between 1.5-6.5 wt% was determined as the saturation region. In this region, the change in ρ_0/ρ ratio was nearly the same for both polymers.

When comparing the block size effect on electrical conductivity, it can be seen that SEBS-S with a lower EB content had lower volume resistivity values. The difference wasn't drastic as CB filled samples. In other words, the block ratio of polymers wasn't so critical for VGCNF based nanocomposites.

Table 4.3. Volume resistivity and ρ_0/ρ values of both SEBS as a function of VGCNF [26]

Filler Concentration (wt%)	Volume Resistivity (ρ) (ohm.cm)		ρ_0/ρ (ohm.cm)/(ohm.cm)	
	SEBS-M	SEBS-S	SEBS-M	SEBS-S
0	1.09E+17	4.25E+17	1.00E+00	1.00E+00
0.5	5.19E+16	1.52E+16	2.10E+00	2.80E+01
1	2.92E+16	5.56E+15	3.73E+00	7.64E+01
1.5	1.19E+08	9.07E+06	9.16E+08	4.69E+10
3.5	1.70E+07	9.50E+06	6.41E+09	4.47E+10
5	3.53E+06	3.44E+06	3.09E+10	1.24E+11
6.5	9.73E+05	1.23E+06	1.12E+11	3.46E+11

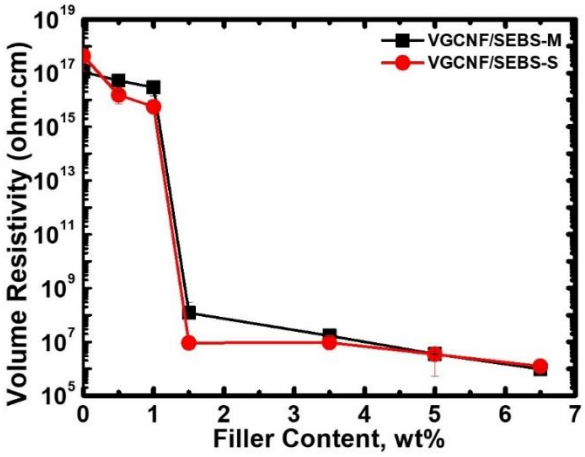

Figure 4.8. Percolation graph of VGCNF filled composites [26]

4.2.3 Mechanical characterization

In order to analyze the mechanical properties of the samples, at least 3 samples for each group were tested with a test speed of 100 mm/min and the distance between grips with 15 mm. As can be seen from Figure 4.9, all thermoplastic elastomer-based composites showed expected stress-strain behavior. VGCNF filled composites had a tensile strain up to 1080% which was higher than neat polymer matrixes. Tensile strength values of SEBS were increased up to 3.5 wt% filler content and then decreased. SEBS-S, having high S content, showed higher tensile strength values. With the addition of nanofibers, both SEBS showed a similar trend Figure 4.10. The aspect ratio of VGCNF is more than 150 μm and the length of the nanofibers is changing around 20-120 μm. The difference in mechanical properties can be derived from the dispersion of nanofibers. When compared to the VGCNF based samples, the tensile strain and tensile strength values were found higher for CB-based composites. It was related to the aspect ratio of the fillers.

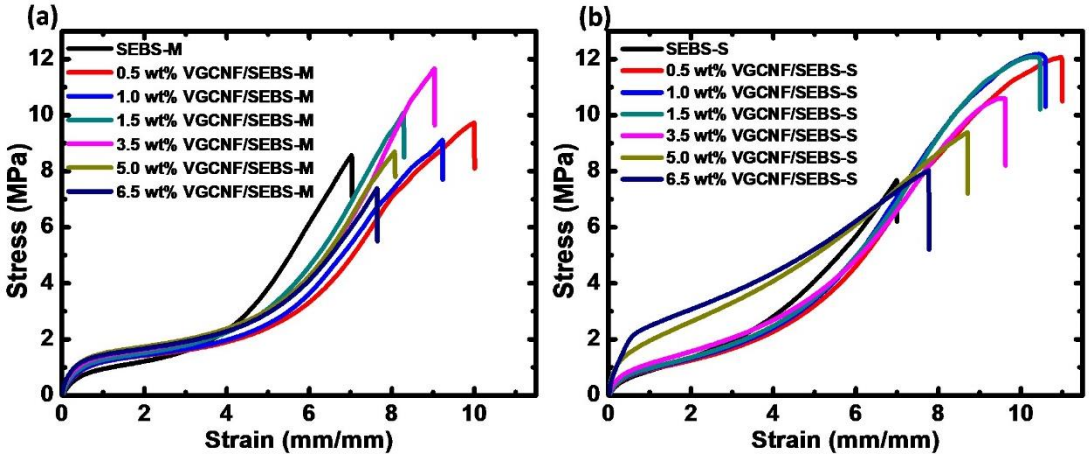

Figure 4.9. Stress-strain curves of (a) VGCNF/SEBS-M and (b) VGCNF/SEBS-S [26]

Table 4.4. Average tensile strength, elastic modulus, and tensile strain values of VGCNF filled SEBS-M and SEBS-S based nanocomposites (SD: Standart Deviation) [26]

Sample	Tensile Strength (MPa)	Normalized Tensile Strength (σ/σ_{SEBS})	Elastic Modulus (MPa)	Normalized Elastic Modulus (E/E_{SEBS})	Tensile Strain (%)	Normalized Tensile Strain ($\varepsilon/\varepsilon_{SEBS}$)
SEBS-M						
SEBS-M	7.50	1.00	2.12	1.00	735.11	1.00
0.5 wt% VGCNF	8.51	1.13	2.29	1.08	901.94	1.23
1.0 wt% VGCNF	8.65	1.15	2.37	1.12	928.87	1.26
1.5 wt% VGCNF	9.88	1.32	2.40	1.13	848.78	1.15
3.5 wt% VGCNF	9.90	1.32	2.81	1.33	824.29	1.12
5.0 wt% VGCNF	8.61	1.15	3.13	1.48	806.99	1.10
6.5 wt% VGCNF	7.88	1.05	3.24	1.53	843.03	1.15
SEBS-S						
SEBS-S	7.66	1.00	1.71	1.00	735.55	1.00
0.5 wt% VGCNF	10.73	1.40	1.85	1.08	1080.18	1.47
1.0 wt% VGCNF	11.54	1.51	2.08	1.22	1057.80	1.44
1.5 wt% VGCNF	11.71	1.53	2.16	1.26	1002.91	1.36
3.5 wt% VGCNF	10.87	1.42	2.31	1.35	995.52	1.35
5.0 wt% VGCNF	10.18	1.33	2.93	1.71	930.09	1.26
6.5 wt% VGCNF	8.81	1.15	3.01	1.76	865.39	1.18

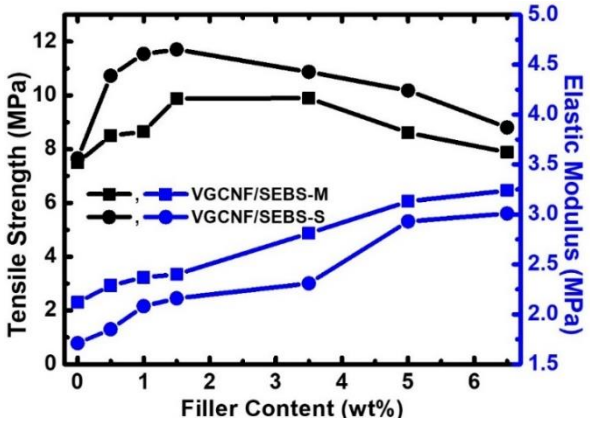

Figure 4.10. Tensile strength and elastic modulus of SEBS-M and SEBS-S as a function of VGCNF loading [26]

4.2.4 Electromechanical characterization

In order to analyze the sensing properties, the samples were chosen from saturation region. 5 and 6.5 wt% of nanofiber filled sensors were investigated under the test speed of 5 mm/min and deformation rate of 20% strain as a function of filler concentration and polymer type. In order to understand the cyclic stability, 50 cycles were carried out (Figure 4.11a) and the initial 5 cycles can be seen from Figure 4.11b. The graph showed the normalized resistance values of the cycles. Under given test conditions, the stability of the sensors was good for 50 cycles. However, the cyclic behavior of SEBS-M was more stable. After the 10th cycle, SEBS-S showed higher stability. The signal of 5 wt% VGCNF/SEBS-M had noisy data. In comparison to SEBS-M and SEBS-S, SEBS-S showed higher sensitivity due to its high EB block ratio. In terms of filler concentration, the normalized resistance values of the sensor with lower filler concentration had higher sensitivity, resulting from the density of conductive network.

The cyclic stability and sensitivity of the sensors were also seen in Figure 4.12. The graph represented GF values depending on the cycle count for all samples. The stabilization of SEBS-S sensors after the 10th cycle can be observed in this graph easily. The highest sensitivity value belonged to 5 wt% VGCNF/SEBS-S under the same conditions.

When the value was compared with the same filler content CB/SEBS-S, which is the sensor with the highest sensitivity values among the CB-based composites, the GF of the VGCNF-filled sensor showed a higher value. It was related to the aspect ratio of

nanoparticles and nanofibers. The aspect ratio of CB was around 1, while VGCNF was more than 150. Thanks to the high aspect ratio of VGCNF, the percolation was determined at lower filler concentration and the conductive network density was lower than CB-based ones for the same concentration. Besides, the conductive network of VGCNF based nanocomposites depended on rotation, alignment, translation, and reorientation under a given deformation rate because of its fibrous structure. On the other hand, CB shows spherical particles and its movement under deformation is limited, in comparison to VGCNF.

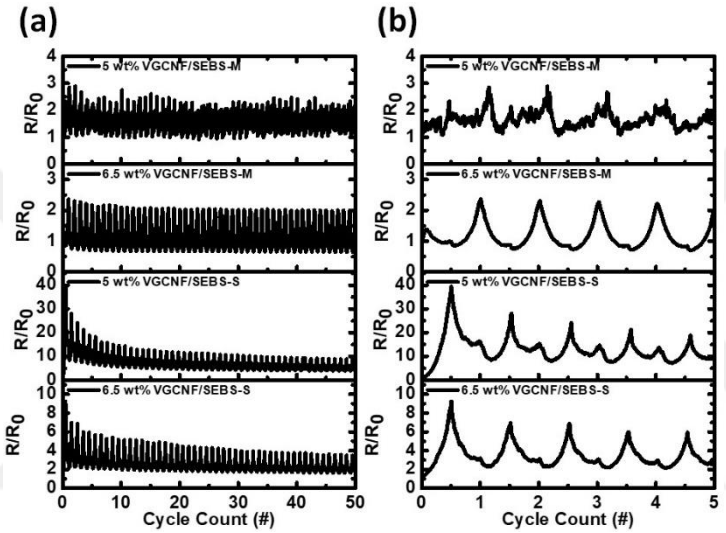

Figure 4.11. Normalized resistance values of 5 and 6.5 wt% VGCNF/SEBS and SEBS-S based on cycle count (a) 50 cycles, and (b) first 10 cycles [26]

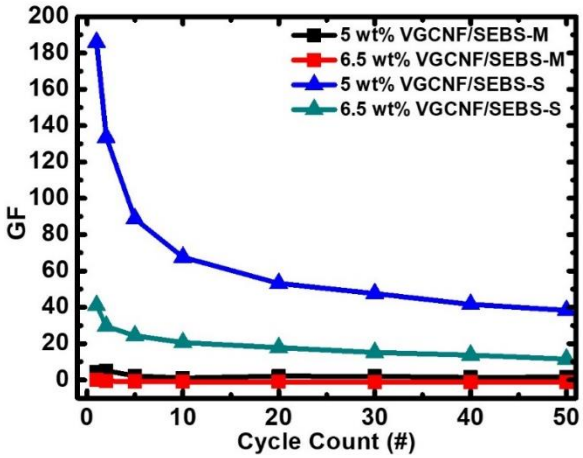

Figure 4.12. GF values of 5 and 6.5 wt% VGCNF/SEBS and SEBS-S samples [26]

4.3 CB-VGCNF/SEBS Piezoresistive Strain Sensors

4.3.1 Morphological characterization

The morphology of the hybrid filler based nanocomposites were analyzed by FESEM. The samples were chosen regarding the percolation graph. For SEBS-M and SEBS-S, 0.5 (insulation region), 3.5 (percolation region), and 6.5 (saturation region) wt% CB-VGCNF based samples were analyzed. In Figure 4.13a and 4.13b, dark grey parts show the electrically insulating SEBS matrix, and light grey parts represent both conductive filler materials. Hybrid filler-based composites were also showed good dispersion and interface. With the increasing filler concentration, the formation of the conductive network can be seen easily. The high magnification images of 6.5 wt% hybrid filler-based SEBS-M and SEBS-S can be seen in Figure 4.13c and 4.13d. The dispersion of hybrid fillers was more homogenous in the SEBS-M matrix, while in the SEBS-S matrix, VGCNF flocks were observed.

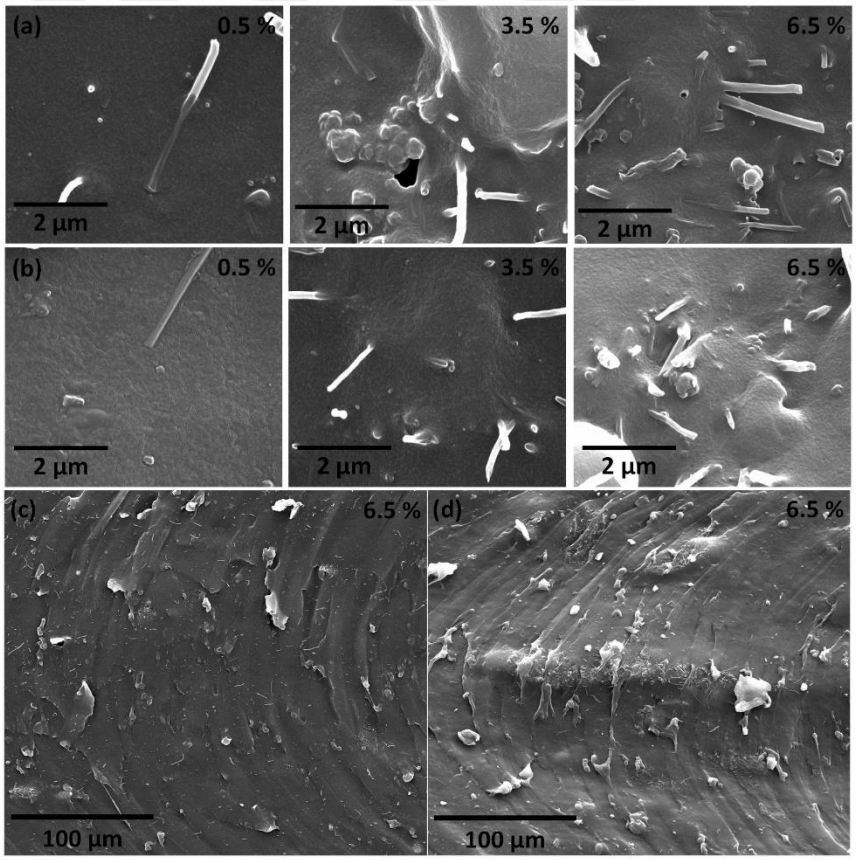

Figure 4.13. FESEM images of (a) CB-VGCNF/SEBS-M, (b) CB-VGCNF /SEBS-S, (c), and (d) High magnification images of SEBS-M and SEBS-S, respectively [26]

4.3.2 Electrical characterization

In order to determine the percolation threshold, the volume resistivity of CB-VGNCF filled SEBS-M and SEBS-S nanocomposites were measured depending on filler loading, which was varied from 0 to 6.5 wt%. The percolation graph and normalized volume resistivity can be seen in Figure 4.14 and Table 4.5. The three regions (insulation, percolation, and saturation) were observed for both polymers. For SEBS-M, the insulating region was determined 0-1.5 wt% hybrid filler loading. In this region, the plateau was observed in the percolation graph and ρ_0/ρ was almost the same with neat polymer (Table 4.5). Percolation threshold was determined between 1.5-3.5 wt% filled nanocomposites. A significant decrease was observed from Figure 4.14 and the decrease in ρ_0/ρ ratio was eight order of magnitude (Table 4.5). The region above 3.5 wt% CB-VGCNF was called saturation since a slight change was observed in volume resistivity. On the other hand, insulation, percolation, and saturations regions were determined as 0-1, 1-1.5, and 1.5-6.5 wt% CB-VGCNF/SEBS-S, respectively.

For both hybrid filler-based nanocomposites, percolation graphs were obtained between CB and VGCNF filled composites. It was concluded that with the addition of VGCNF, lower volume resistivity values were observed. Also, with the hybrid filler system, the new junctions (CB-VGCNF) were obtained, as well as CB-CB, and VGCNF-VGCNF junctions. SEBS with a lower EB content showed a lower percolation threshold as CB and VGCNF filled composites. As previously mentioned, CB preferably dispersed in the EB phase and it was confirmed by FESEM images (Figure 4.13c and 4.13d). As can be seen from these images, homogenous dispersion was obtained with SEBS-M, and some flocks were observed SEBS-S based composites.

Table 4.5. Volume resistivity and ρ_0/ρ values of both SEBS as a function of CB-VGCNF [26]

Filler Concentration (wt%)	Volume Resistivity (ρ) (ohm.cm)		ρ_0/ρ (ohm.cm)/(ohm.cm)	
	SEBS-M	SEBS-S	SEBS-M	SEBS-S
0	1.09E+17	4.25E+17	1.00E+00	1.00E+00
0.5	4.71E+16	1.56E+16	2.31E+00	2.72E+01
1	4.43E+16	1.50E+16	2.46E+00	2.83E+01
1.5	1.75E+16	1.93E+14	6.23E+00	2.20E+03
3.5	1.41E+08	9.89E+06	7.73E+08	4.30E+10
5	1.27E+07	2.56E+06	8.58E+09	1.66E+11
6.5	1.40E+06	8.56E+05	7.79E+10	4.96E+11

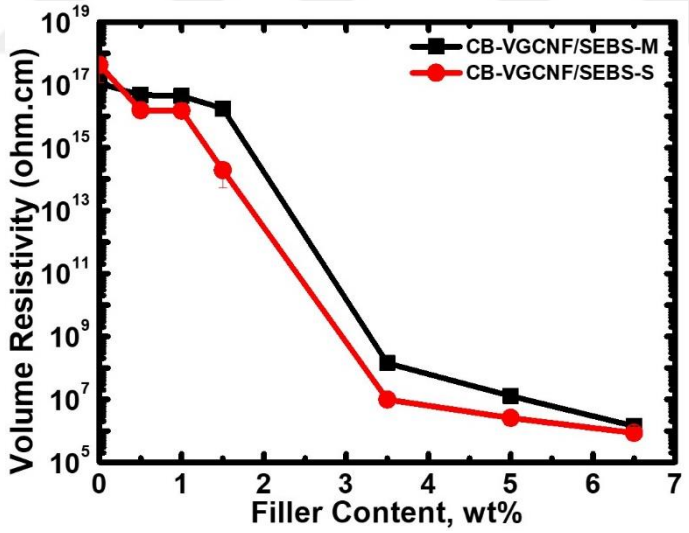

Figure 4.14. Percolation graph of CB-VGCNF filled composites [26]

4.3.3 Mechanical characterization

In order to characterize the mechanical properties of the hybrid composites, the test speed was adjusted to 100 mm/min and at least 3 samples for each group were tested. All thermoplastic elastomer-based samples showed classical stress-strain behavior (Figure 4.15) and average and normalized values of tensile strength, tensile strain, and elastic modulus can be seen from Table 4.6. Tensile strain values of the composites increased up to 1102% with the addition of CB-VGCNF. For SEBS-M, tensile strength increased up to 6.5 wt% filler content, while for SEBS-S, the value decreased after 1.5 wt% filler concentration. In terms of elastic modulus, samples showed similar character (Figure 4.16). The drastic increase in elastic modulus can be seen 5 wt% CB-VGCNF/SEBS-S. When compared to single fillers, the increment in tensile strength, tensile strain, and elastic modulus was obtained generally with the hybrid fillers.

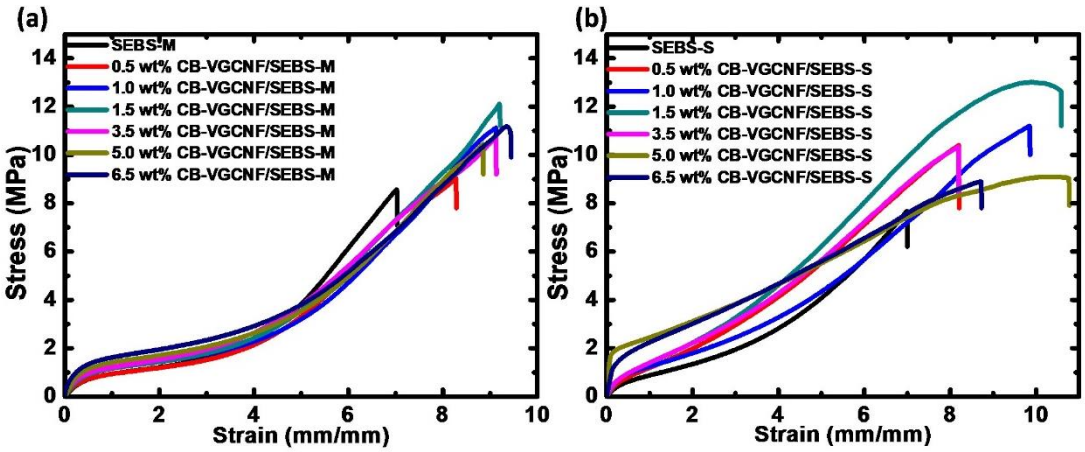

Figure 4.15. Stress-strain curves of (a) CB-VGCNF/SEBS-M and (b) CB-VGCNF/SEBS-S [26]

Table 4.6. Average tensile strength, elastic modulus, and tensile strain values of CB-VGCNF filled nanocomposites (SD: Standart Deviation) [26]

Sample	Tensile Strength (MPa)	Normalized Tensile Strength (σ/σ_{SEBS})	Elastic Modulus (MPa)	Normalized Elastic Modulus (E/E_{SEBS})	Tensile Strain (%)	Normalized Tensile Strain ($\varepsilon/\varepsilon_{SEBS}$)
SEBS-M						
SEBS-M	7.50	1.00	2.12	1.00	735.11	1.00
0.5 wt% CB-VGCNF	8.99	1.20	2.13	1.00	815.03	1.11
1.0 wt% CB-VGCNF	9.32	1.24	2.30	1.08	864.20	1.18
1.5 wt% CB-VGCNF	9.47	1.26	2.41	1.14	824.40	1.12
3.5 wt% CB-VGCNF	9.49	1.27	2.74	1.29	852.36	1.16
5.0 wt% CB-VGCNF	10.59	1.41	2.78	1.31	875.8	1.19
6.5 wt% CB-VGCNF	11.55	1.54	2.85	1.34	964.05	1.31
SEBS-S						
SEBS-S	7.66	1.00	1.71	1.00	735.55	1.00
0.5 wt% CB-VGCNF	10.60	1.38	1.92	1.12	962.79	1.31
1.0 wt% CB-VGCNF	10.72	1.40	1.95	1.14	914.88	1.24
1.5 wt% CB-VGCNF	10.82	1.41	2.30	1.35	918.34	1.25
3.5 wt% CB-VGCNF	9.55	1.25	2.35	1.37	905.75	1.23
5.0 wt% CB-VGCNF	9.76	1.27	3.50	2.05	1102.61	1.50
6.5 wt% CB-VGCNF	9.07	1.18	3.65	2.13	840.97	1.14

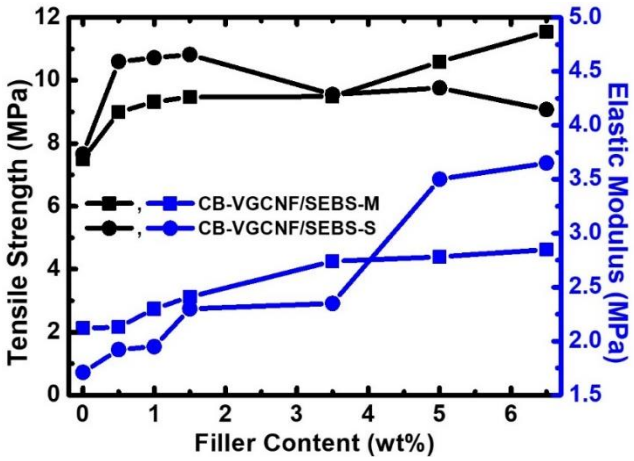

Figure 4.16. Tensile strength and elastic modulus of SEBS-M and SEBS-S as a function of CB-VGCNF loading [26]

4.3.4 Electromechanical characterization

In order to investigate sensing properties, samples consisting of 5 and 6.5 wt% filler content and 3.5, 5, and 6.5 wt% filler were chosen depending on electrical properties for SEBS-M and SEBS-S based composites, respectively. For SEBS-M, 3.5 wt% CB-VGCNF filled sample was in the percolation region with a resistivity value of 1.41E+08 and the data couldn't obtain with the four-probe measurement system, thus its electromechanical properties didn't perform. The test speed (5 mm/min) and deformation (20%) were kept the same for other samples. In order to analyze the cyclic stability, 50 cycles were performed (Figure 4.17a) and in detail, the first 5 cycles were given in Figure 4.17b. All samples showed cyclic stability but the stability of SEBS-M was higher than reported composites, consisting of single fillers. The noisy signal couldn't be observed thanks to the incorporation of two different fillers. The higher normalized resistance values were obtained with the samples SEBS, having S content as single filler systems. With the addition of filler, normalized resistance values decreased and the highest GF (333) was obtained with the sample 3.5 wt% CB-VGCNF/SEBS-S. As mentioned before, it was related to the conductive network density. It can be reported that with the addition of hybrid filler, new conductive network junctions were formed (CB-VGCNF), as well as CB-CB, and VGCNF-VGCNF, and consequently smooth data, higher stability, and higher sensitivity were obtained.

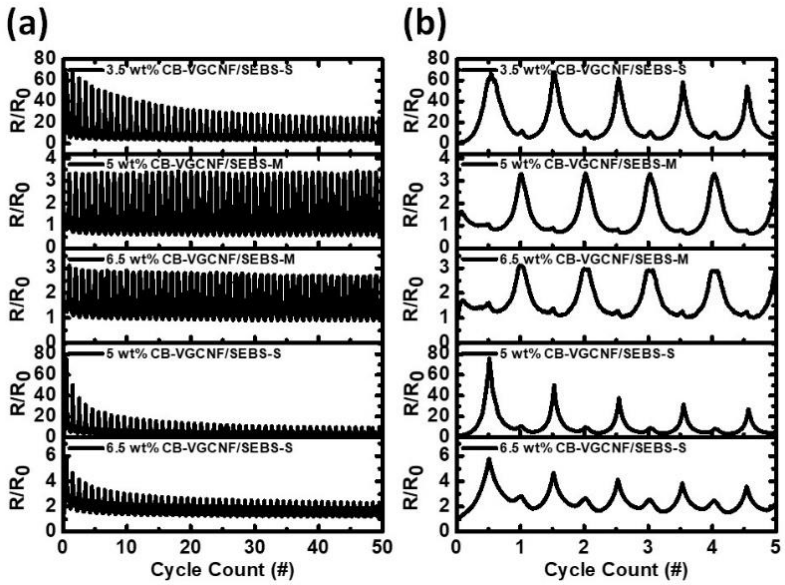

Figure 4.17. Normalized resistance values of 5 and 6.5 wt% CB-VGCNF/SEBS-M and 3.5, 5, and 6.5 wt% CB-VGCNF/SEBS-S based on cycle count (a) 50 cycles, and (b) first 10 cycles [26]

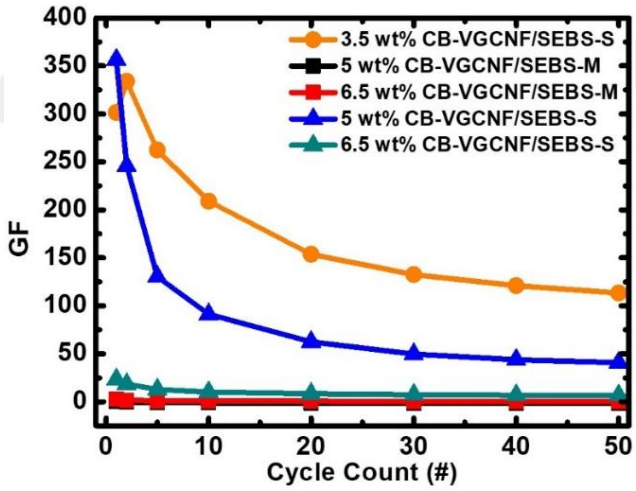

Figure 4.18. GF values of 5 and 6.5 wt% CB-VGCNF/SEBS-M and 3.5, 5, and 6.5 wt% CB-VGCNF/SEBS-S samples [26]

4.4 Textile Based Hybrid Piezoresistive Strain Sensor

In order to investigate the properties of the sensors as an electronic textile, sample were coated on the fabric. SEBS-S with a filler content of 4 wt% were chosen in order to get more accurate data from four-probe measurement system.

4.4.1 Morphological characterization

In order to understand the morphology of the fabric-based hybrid piezoresistive strain sensor, SEM analysis was carried out. The layered structure, filler orientation, filler-matrix orientation, and interaction can be seen from Figure 4.19 at different magnifications. The parameters are important in terms of electrical and electromechanical characteristics. The surface fibers of knitted fabric could be seen and the interface between coating and fabric was good. The dark parts represented SEBS as a continuous phase, and hybrid fillers could be seen easily in light parts because of their high electrical conductivity. The fillers were homogenously dispersed without any orientation.

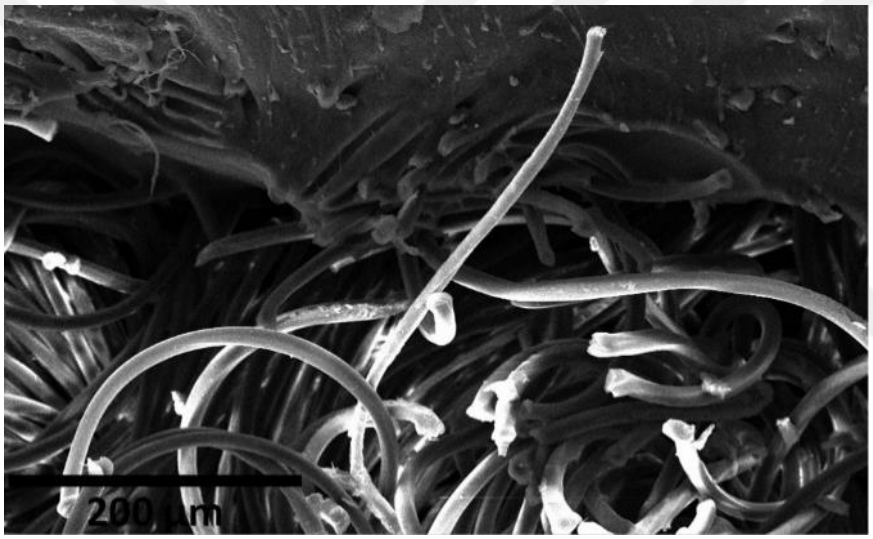

Figure 4.19. FESEM image of textile based hybrid piezoresistive strain sensor (Scale bar: 200 µm)

4.4.2 Electromechanical characterization

The textile-based hybrid sensor was performed different conditions (test speed of 5 and 50 mm/min, strain (5, 10, 20, 25, 30 %, and stepwise tests with a speed of 5 and 50 mm/min and 5, 10, 20, 25% strain). In the study, the result of 5 mm/min and 20% strain was given (Figure 4.20). 50 cycles were carried out (Figure 4.20a) and the initial 5 cycles were also given Figure 4.20b. For the layered structure of the sensor, the interaction between coating and fabric is important, especially in terms of electrical and electromechanical properties. The good interface can be seen in the previous section (Figure 4.19). Thanks to the interface, textile-based hybrid piezoresistive strain sensors showed as high stability as film sensors. The smooth data was also obtained due to the fabric. GF was obtained ~108 for the first cycle and for 50 cycles was between 108-75. The sensitivity wasn't as high as single/hybrid film sensors because fabric structure probably limited mobility of the sensor.

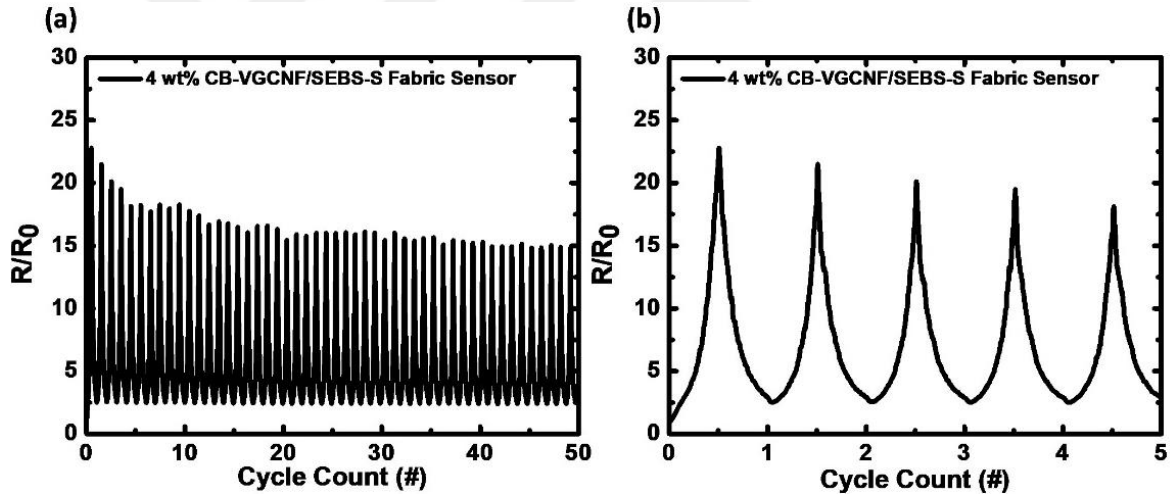

Figure 4.20. Normalized resistance values of 4 wt% CB-VGCNF/SEBS-S based on cycle count (a) 50 cycles, and (b) first 10 cycles

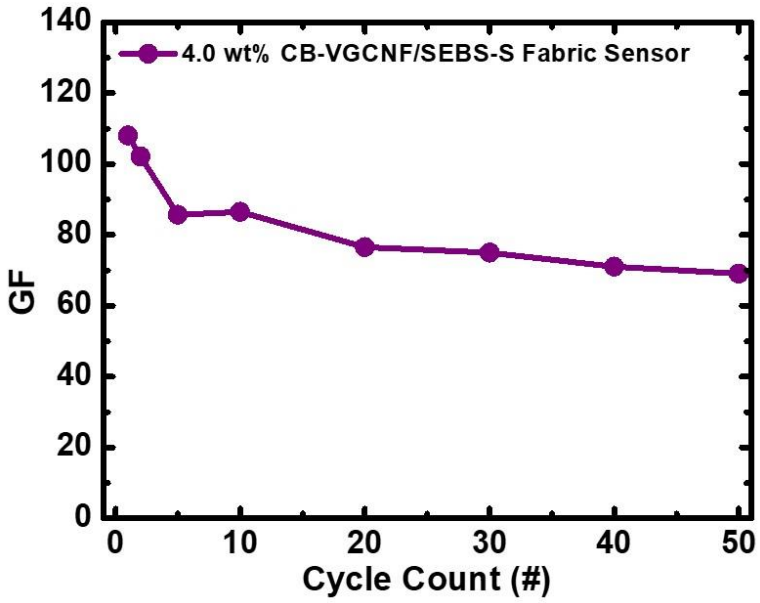

Figure 4.21. GF values of 4 wt% CB-VGCNF/SEBS-S sample

5. CONCLUSIONS AND FUTURE SUGGESTIONS

In the study, piezoresistive strain sensors were designed and fabricated. CB and VGCNF filled composites were produced. As a novelty, the mixture of CB and VGCNF were used as a hybrid electrically conductive filler material. Besides, thermoplastic elastomers with two different block ratios were used. In the first step, the nanocomposites were fabricated by solution casting and then compression molding. In order to obtain homogenous nanocomposites, the fillers were dispersed in polymers by using the high shear planetary mixer. The properties of CB, VGCNF, CB-VGCNF filled nanocomposites were investigated in terms of morphological, electrical, mechanical, and electromechanical properties. For the morphological analysis, all samples showed homogeneity thanks to the high shear mixing step. In terms of electrical properties, CB showed high percolation concentration because of its low aspect ratio, while the percolation threshold of VGCNF was relatively low thanks to its high aspect ratio. With incorporation of CB and VGCNF, the new junctions (CB-VGCNF) formed as well as CB-CB and VGCNF-VGCNF and percolation threshold was obtained between CB and VGCNF filled composites. The study mainly focused on electromechanical behavior as well as electrical properties, depending on filler type/concentration/aspect ratio/geometry, and polymer type. In terms of electromechanical characterization, samples were chosen by considering percolation behavior. For the characterization of electromechanical properties of single and hybrid filler filled sensors, cyclic stability, noisiness of cycle, and sensitivity were investigated based on 50 cycles under 20% strain with a 5 mm/min test speed. The sensitivity of the sensors was as follows; CB filled < VGCNF filled < CB- VGCNF filled sensors at 5 wt% filler concentration. The highest sensitivity was reported for the sensor 3.5 wt% CB-VGCNF/SEBS-S. In terms of filler concentration for the same polymer matrix, higher sensitivity was generally obtained at lower filler concentration. That behavior was related to the percolation behavior and density of conducting network.

In the next step, the sensor, 4 wt% CB-VGCNF/SEBS-S, was coated on the fabric and its electromechanical properties were also investigated as nanocomposites. As a result, a piezoresistive strain sensor, consisting of a hybrid filler, was developed for the first time in the literature. Electrically conductive nanocomposites, which were produced

from electrically conductive fillers such as single or hybrid materials, can be used as wearable electronics in order to monitor human motions. Future studies will focus on fabrication of different hybrid flexible electronics at different mixture ratio of CB: VGCNF with different sensor dimensions. Also, the flexible electronic developed in this work can be evaluated as pressure, temperature, chemical, or gas sensors.

REFERENCES

[1] W. S. Wong and A. Salleo, Eds., *Flexible Electronics*, vol. 11. Boston, MA: Springer US, 2009.

[2] J. Fraden, *Handbook of Modern Sensors*. Springer New York, 2010.

[3] M. S. Cetin, O. Toprakci, and H. A. K. Toprakci, "Flexible Piezoresistive Strain Sensors Based on Carbonaceous Filler/Thermoplastic Elastomer Composites," in *Theory and Research in Engineering II*, vol. 2, Gece Publishing, 2020, pp. 215–236.

[4] T. Kenny, W. Kester, and G. C. Low, "Strain Gages," in *Sensor Technology Handbook*, Newnes, 2005, pp. 501–529.

[5] W. Wu, "Stretchable electronics: functional materials, fabrication strategies and applications," *Science and Technology of Advanced Materials*, vol. 20, no. 1, pp. 187–224, 2019.

[6] W.-T. Park, *Piezoresistivity*. Springer, Dordrecht, 2016.

[7] J. S. Wilson, *Sensor Technology Handbook*. Elsevier Inc., 2005.

[8] A. S. Dahiya, Y. Kumaresan, O. Ozioko, M. Ntagios, and R. Dahiya, *Soft Sensors for Electronic Skin*. Elsevier, 2021.

[9] X. Fu, M. Ramos, A. M. Al-Jumaily, A. Meshkinzar, and X. Huang, "Stretchable strain sensor facilely fabricated based on multi-wall carbon nanotube composites with excellent performance," *Journal of Materials Science*, vol. 54, no. 3, pp. 2170–2180, 2019.

[10] Y. Jung *et al.*, "Wearable piezoresistive strain sensor based on graphene-coated three-dimensional micro-porous PDMS sponge," *Micro and Nano Systems Letters*, vol. 7, no. 1, pp. 1–9, 2019.

[11] J. Narongthong, A. Das, H. H. Le, S. Wießner, and C. Sirisinha, "An efficient highly flexible strain sensor: Enhanced electrical conductivity, piezoresistivity and flexibility of a strongly piezoresistive composite based on conductive carbon black and an ionic liquid," *Composites Part A: Applied Science and Manufacturing*, vol. 113, pp. 330–338, Oct. 2018.

[12] A. Georgopoulou, S. Michel, B. Vanderborght, and F. Clemens, "Piezoresistive sensor fiber composites based on silicone elastomers for the monitoring of the position of a robot arm," *Sensors and Actuators A: Physical*, vol. 318, p. 112433, 2021.

[13] A. Georgopoulou and F. Clemens, "Piezoresistive Elastomer-Based Composite Strain Sensors and Their Applications," *ACS Applied Electronic Materials*, vol. 2, no. 7, pp. 1826–1842, 2020.

[14] W. Zhang, Q. Liu, and P. Chen, “Flexible strain sensor based on carbon black/silver nanoparticles composite for human motion detection,” *Materials*, vol. 11, no. 10, 2018.

[15] P. Costa, S. Gonçalves, H. Mora, S. A. C. Carabineiro, J. C. Viana, and S. Lanceros-Mendez, “Highly Sensitive Piezoresistive Graphene-Based Stretchable Composites for Sensing Applications,” *ACS Applied Materials & Interfaces*, vol. 11, no. 49, pp. 46286–46295, Dec. 2019.

[16] M. Melnykowycz, B. Koll, D. Scharf, and F. Clemens, “Comparison of Piezoresistive Monofilament Polymer Sensors,” *Sensors*, vol. 14, no. 1, pp. 1278–1294, Jan. 2014.

[17] B. F. Gonçalves *et al.*, “Green solvent approach for printable large deformation thermoplastic elastomer based piezoresistive sensors and their suitability for biomedical applications,” *Journal of Polymer Science Part B: Polymer Physics*, vol. 54, no. 20, pp. 2092–2103, 2016.

[18] M. Melnykowycz, M. Tschudin, and F. Clemens, “Piezoresistive Soft Condensed Matter Sensor for Body-Mounted Vital Function Applications,” *Sensors*, vol. 16, no. 3, p. 326, Mar. 2016.

[19] P. Costa *et al.*, “Effect of carbon nanotube type and functionalization on the electrical, thermal, mechanical and electromechanical properties of carbon nanotube/styrene–butadiene–styrene composites for large strain sensor applications,” *Composites Part B: Engineering*, vol. 61, pp. 136–146, 2014.

[20] A. Poudel *et al.*, “Processing of nanocomposites using supercritical fluid assisted extrusion for stress/strain sensing applications,” *Composites Part B: Engineering*, vol. 165, pp. 397–405, 2019.

[21] A. Turgut, M. O. Tuhin, O. Toprakci, M. A. Pasquinelli, R. J. Spontak, and H. A. K. Toprakci, “Thermoplastic Elastomer Systems Containing Carbon Nanofibers as Soft Piezoresistive Sensors,” *ACS Omega*, vol. 3, no. 10, pp. 12648–12657, Oct. 2018.

[22] E. Bilotti, H. Zhang, H. Deng, R. Zhang, Q. Fu, and T. Peijs, “Controlling the dynamic percolation of carbon nanotube based conductive polymer composites by addition of secondary nanofillers: The effect on electrical conductivity and tuneable sensing behaviour,” *Composites Science and Technology*, vol. 74, pp. 85–90, 2013.

[23] C. Cochrane, V. Koncar, M. Lewandowski, and C. Dufour, “Design and development of a flexible strain sensor for textile structures based on a conductive polymer composite,” *Sensors*, vol. 7, no. 4, pp. 473–492, 2007.

[24] C. Mattmann, F. Clemens, and G. Tröster, “Sensor for Measuring Strain in Textile,” *Sensors 2008, Vol. 8, Pages 3719-3732*, vol. 8, no. 6, pp. 3719–3732, Jun. 2008.

[25] F. J. Clemens *et al.*, “Development of Piezoresistive Fiber Sensors, Based on

Carbon Black Filled Thermoplastic Elastomer Compounds, for Textile Application," *Advances in Science and Technology*, vol. 80, pp. 7–13, Sep. 2013.

[26] M. S. Cetin and H. A. Karahan Toprakci, "Flexible electronics from hybrid nanocomposites and their application as piezoresistive strain sensors," *Composites Part B: Engineering*, vol. 224, p. 109199, Nov. 2021.

[27] D. D. L. Chung, "A critical review of piezoresistivity and its application in electrical-resistance-based strain sensing," *Journal of Materials Science*, vol. 55, no. 32, pp. 15367–15396, 2020.

[28] F. Boussu, N. Trifigny, C. Cochrane, and V. Koncar, "Fibrous sensors to help the monitoring of weaving process," in *Smart Textiles and Their Applications*, Woodhead Publishing, 2016, pp. 375–400.

[29] D. De Rossi, F. Carpi, F. Lorussi, E. P. Scilingo, A. Tognetti, and R. Paradiso, *Electroactive fabrics and wearable man–machine interfaces*. Woodhead Publishing, 2005.

[30] Y. Sun, T. Nishida, and S. E. Thompson, "Piezoresistive Strain Sensors," in *Strain Effect in Semiconductors*, Springer, Boston, MA, 2010, pp. 267–290.

[31] D. Hazarika and N. Karak, "Fundamentals of polymeric nanostructured materials," *Advances in Polymeric Nanomaterials for Biomedical Applications*, pp. 1–40, 2021.

[32] L. Duan *et al.*, "Designing formulation variables of extrusion-based manufacturing of carbon black conductive polymer composites for piezoresistive sensing," *Composites Science and Technology*, vol. 171, pp. 78–85, 2019.

[33] W. Obitayo and T. Liu, "A review: Carbon nanotube-based piezoresistive strain sensors," *Journal of Sensors*, vol. 2012, 2012.

[34] Alamusi, N. Hu, H. Fukunaga, S. Atobe, Y. Liu, and J. Li, "Piezoresistive Strain Sensors Made from Carbon Nanotubes Based Polymer Nanocomposites," *Sensors (Basel, Switzerland)*, vol. 11, no. 11, p. 10691, Nov. 2011.

[35] P. Costa, A. Ferreira, V. Sencadas, J. C. Viana, and S. Lanceros-Méndez, "Electro-mechanical properties of triblock copolymer styrene–butadiene–styrene/carbon nanotube composites for large deformation sensor applications," *Sensors and Actuators A: Physical*, vol. 201, pp. 458–467, 2013.

[36] X. Yang, L. Sun, C. Zhang, B. Huang, Y. Chu, and B. Zhan, "Modulating the sensing behaviors of poly(styrene-ethylene-butylene-styrene)/carbon nanotubes with low-dimensional fillers for large deformation sensors," *Composites Part B: Engineering*, vol. 160, pp. 605–614, 2019.

[37] S. Pan *et al.*, "A highly stretchable strain sensor based on CNT/graphene/fullerene-SEBS," *RSC Advances*, vol. 10, no. 19, pp. 11225–11232, 2020.

[38] C. W. Nan, “Physics of inhomogeneous inorganic materials,” *Progress in Materials Science*, vol. 37, no. 1, pp. 1–116, Jan. 1993.

[39] Q. Xue and J. Sun, “Electrical conductivity and percolation behavior of polymer nanocomposites,” *Polymer Nanocomposites: Electrical and Thermal Properties*, pp. 51–82, Jan. 2016.

[40] T. J. Fiske, H. S. Gokturk, and D. M. Kalyon, “Percolation in magnetic composites,” *Journal of Materials Science*, vol. 32, no. 20, pp. 5551–5560, 1997.

[41] *Fundamentals of Polymer Matrix Composites Containing CNTs*. William Andrew Publishing, 2015.

[42] M. Weber and M. R. Kamal, “Estimation of the volume resistivity of electrically conductive composites,” *Polymer Composites*, vol. 18, no. 6, pp. 711–725, 1997.

[43] E. P. Mamunya, V. V. Davidenko, and E. V. Lebedev, “Effect of polymer-filler interface interactions on percolation conductivity of thermoplastics filled with carbon black,” *Composite Interfaces*, vol. 4, no. 4, pp. 169–176, 1997.

[44] B. Alemour, O. Badran, and M. R. Hassan, “A review of using conductive composite materials in solving lightening strike and ice accumulation problems in aviation,” *Journal of Aerospace Technology and Management*, vol. 11, 2019.

[45] Y. D. Shi, J. Li, Y. J. Tan, Y. F. Chen, and M. Wang, “Percolation behavior of electromagnetic interference shielding in polymer/multi-walled carbon nanotube nanocomposites,” *Composites Science and Technology*, vol. 170, pp. 70–76, 2019.

[46] R. Bhatia, K. Kumari, R. Rani, A. Suri, U. Pahuja, and D. Singh, “A critical review of experimental results on low temperature charge transport in carbon nanotubes based composites,” *Reviews in Physics*, vol. 3, pp. 15–25, 2018.

[47] J. Zavickis, A. Linarts, and M. Knite, “The downshift of the electrical percolation threshold in polyisoprene-nanostructured carbon composites,” *Energetika*, vol. 57, no. 1, 2011.

[48] T. Khan, M. S. Irfan, M. Ali, Y. Dong, S. Ramakrishna, and R. Umer, “Insights to low electrical percolation thresholds of carbon-based polypropylene nanocomposites,” *Carbon*, vol. 176, pp. 602–631, 2021.

[49] M. Mazaheri, J. Payandehpeyman, and S. Jamasb, “Modeling of Effective Electrical Conductivity and Percolation Behavior in Conductive-Polymer Nanocomposites Reinforced with Spherical Carbon Black,” *Applied Composite Materials*, 2021.

[50] Y. Zheng *et al.*, “Conductive thermoplastic polyurethane composites with tunable piezoresistivity by modulating the filler dimensionality for flexible strain sensors,” *Composites Part A: Applied Science and Manufacturing*, vol. 101, pp. 41–49, 2017.

[51] L. Duan, D. R. D'Hooge, M. Spoerk, P. Cornillie, and L. Cardon, "Facile and Low-Cost Route for Sensitive Stretchable Sensors by Controlling Kinetic and Thermodynamic Conductive Network Regulating Strategies," *ACS Applied Materials and Interfaces*, vol. 10, no. 26, pp. 22678–22691, 2018.

[52] S. Pavlovsky and A. Siegmann, "Chemical sensing materials. I. Electrically conductive SEBS copolymer systems," *Journal of Applied Polymer Science*, vol. 113, no. 5, pp. 3322–3329, 2009.

RESUME

Graduated from primary and high school in Yalova. Then, started the Department of Polymer Engineering at Yalova University and graduated with a degree of the highest ranked student of Yalova University Engineering Faculty in 2019.

Experiences and Awards:

Worked in "Electromechanical Sensing Properties of Flexible Electronics from Functional Polymer Nanocomposites" project as a scholarship student that was supported by TUBITAK 2210-C National Graduate Scholarship Program in High Priority Technological Areas

First prize in "Uşak Üniversitesi TTO 2.Ar-Ge Proje Pazarı" with the project of "Electromechanical Sensing Properties of Flexible Electronics from Functional Polymer Nanocomposites"

PUBLICATIONS AND PRESENTATIONS DERIVED FROM THESIS/DISSERTATION

Publication in a Journal:

M. S. Cetin and H. A. Karahan Toprakci, "Flexible electronics from hybrid nanocomposites and their application as piezoresistive strain sensors," *Composites Part B: Engineering*, vol. 224, p. 109199, Nov. 2021.

Book Chapter:

M. S. Cetin, O. Toprakci, and H. A. K. Toprakci, "Flexible Piezoresistive Strain Sensors Based on Carbonaceous Filler/Thermoplastic Elastomer Composites," in *Theory and Research in Engineering II*, vol. 2, Gece Publishing, 2020, pp. 215–236.

Proceedings:

H. A. Karahan Toprakci, M. S. Cetin, and O. Toprakci, "Hybrid Nanocomposites and Their Stress Sensing Behaviour," Ahi Evran International Conference on Scientific Research Congress, Nov. 2021.

M. S. Cetin, O. Toprakci, and H. A. Karahan Toprakci, "Fabrication of Nanocomposites from Single and Hybrid Fillers and Their Application for Determination Applied Force," Ahi Evran International Conference on Scientific Research Congress, Nov. 2021.

H. A. Karahan Toprakci, M. S. Cetin, and O. Toprakci, "Effects of Filler Geometry on Sensing Behavior of Flexible Nanocomposites," 7th International GAP Mathematics-Engineering-Science and Health Sciences Congress, Nov. 2021.

M. S. Cetin, O. Toprakci, and H. A. Karahan Toprakci, "Investigation of Electromechanical Sensing Properties of Nanofiber Filled Block Copolymer Based Nanocomposites," 7th International GAP Mathematics-Engineering-Science and Health Sciences Congress, Nov. 2021.

H. A. Karahan Toprakci, M. S. Cetin, and O. Toprakci, "Fabrication of Carbon Black and Vapor Grown Carbon Nanofiber Filled Nanocomposites and Investigation of Their Sensing Properties as a Function of Filler Aspect Ratio and Test Speed," II. International Halich Congress on Multidisciplinary Scientific Research, Oct. 2021.

M. S. Cetin and H. A. Karahan Toprakci, “Investigation of Synergistic Effects of Hybrid Fillers on Sensing Properties of Flexible Nanocomposite Strain Sensors,” II. International Halich Congress on Multidisciplinary Scientific Research, Oct. 2021.

M. Ş. Çetin, O. Toprakçı, and H. A. Karahan Toprakçı, “Esnek, Hibrit Elektroniklerin Elektromekanik Algılama Özellikleri ve Tekstil Sensörü Uygulamaları,” Bartın Üniversitesi 4.Ar-Ge Proje Pazarı, Oct. 2021.

M. Ş. Çetin and H. A. Karahan Toprakçı, “Fonksiyonel Polimer Kompozitlerden Üretilen Esnek Elektroniklerin Elektromekanik Algılama Özelliklerinin İncelenmesi,” Uşak Üniversitesi TTO 2.Proje Pazarı, Oct. 2021.

Publication and Patent List:

A. S. Demirel, M. Ş. Çetin, and H. A. Karahan Toprakçı, “Antep Fıstığı Kabuk Atıklarından Esnek Elektronik Üretimi,” Bartın Üniversitesi 4.Ar-Ge Proje Pazarı, Oct. 2021.

İ. Ekiz, M. S. Cetin, and H. A. Karahan Toprakci, “Preparation and Characterization of Poly(Lactic Acid) Blends,” 6. Internatıonal Congress on Engineering and Technology Management, Nov. 2021.

M. S. Cetin, O. Toprakci, O. S. Taskin, A. Aksu, and H. A. K. Toprakci, “Expanded vermiculite-filled flexible polymer composites:,” *Journal of Elastomers & Plastics*, vol. 54, no. 1, pp. 145–168, Jul. 2022.

M. Ş. Çetin, A. S. Demirel, O. Toprakçı, and H. A. Toprakçı Karahan, “Karbonize edilmiş antep fıstığı kabuk atıklarından iletken, esnek polimer kompozit üretimi ve karakterizasyonu,” *Gazi Üniversitesi Mühendislik Mimarlık Fakültesi Dergisi*, vol. 37, no. 2, pp. 711–722, 2022.

O. Toprakci, M. S. Cetin, and H. A. Karahan Toprakci, “Production of Styrene-[ethylene-(ethylene-propylene)]-styrene block copolymer (SEEPS) microfibers by electrospinning,” *Material Science Research India*, vol. 18, no. 1, pp. 27–36, 2021.

H. A. K. Toprakci, M. S. Cetin, and O. Toprakci, “Fabrication of Conductive Polymer Composites from Turkish Hemp-Derived Carbon Fibers and Thermoplastic Elastomers,” *Tekstil ve Muhendis*, vol. 28, no. 121, pp. 32-38., 2021.

O. Toprakci, M. S. Cetin, and H. A. Toprakci Karahan, “ Vermiculite filled polymer composites,” in *Theory and Research in Engineering II*, vol. 1, pp. 125–144, 2020.